PERGAMON

International Journal of Solids and Structures 37 (2000) 3681–3713

INTERNATIONAL JOURNAL OF SOLIDS and STRUCTURES

www.elsevier.com/locate/ijsolstr

Nonlinear thermoelastic analysis of composite panels under non-uniform temperature distribution

A. Barut [a], E. Madenci [a,*], A. Tessler [b]

[a] *Department of Aerospace and Mechanical Engineering, The University of Arizona, Aero Bldg. 16, Tucson, AZ 85721 USA*
[b] *NASA Langley Research Center, MS 240, Hampton, VA 23681-0001, USA*

Received 20 July 1998; in revised form 29 March 1999

Abstract

The response of moderately thick laminated panels experiencing large displacements and rotations under non-uniform thermal loading is investigated through a nonlinear finite element analysis. The present nonlinear thermoelastic analysis incorporates an anisoparametric, doubly curved, shallow shell element that is free of the 'locking' phenomenon. The effects of large displacements and rotations, transverse shear deformations, the coupling between stretching and bending due to shallow geometry, and Duhamel–Neumann-type thermoelastic material anisotropy are included in the element formulation. The equations of equilibrium are derived from the virtual work principle, along with the co-rotational form of the total Lagrangian formulation. A non-uniform temperature field across the shell surface is approximated by piecewise-uniform temperature distributions over individual elements. In the thickness direction, the temperature distribution is approximated linearly. Accuracy of the present analysis is established by comparison with benchmark solutions. The numerical results are presented for various configurations, including cutouts under uniform and non-uniform temperatures. The numerical results demonstrate that the present finite element analysis is computationally robust and efficient.

1. Introduction

External surfaces of modern aerospace structures are constructed from stiffened composite laminates because of their attractive mechanical and thermal properties. In aerospace engineering, minimum-weight design of stiffened panels allows the skin to experience postbuckling behavior before reaching the ultimate loading conditions, provided that the complete compressive load is carried by stiffeners. Also, postbuckling of such components may arise from the compressive stresses induced by a sudden temperature rise on the skin due to aerodynamic heating at supersonic speeds. In this case, the skin

* Corresponding author. Fax: +001-502-621-819.
E-mail address: madenci@aue.arizona.edu (E. Madenci).

0020-7683/00/$ - see front matter
PII: S0020-7683(99)00119-5

temperature becomes higher than that of the stiffeners. Because of this temperature difference, the stiffeners, which are cooler than the panels, will resist the thermal expansion of the panels along the skin-stiffener interface, thus initiating compressive stresses in the skin and, possibly, causing the skin to buckle or to experience large transverse deflections (i.e., a softening–stiffening type of behavior). In order to take advantage of the postbuckling strength of these structural components, it is necessary to perform an analysis that predicts their nonlinear response under both mechanical and thermal loading conditions. In addition to this, the aerospace structures include openings, as well as cracks on the skin, rendering the solution of the problem extremely difficult with existing analytical techniques. Therefore, an analysis based on the finite element method seems to be the most applicable approach to deal with such structures (Tripathy and Rao, 1992).

Gossard et al. (1952) seems to have been the first to investigate the nonlinear behavior of thermally induced structures. By employing the Rayleigh–Ritz and Galerkin methods, they presented solutions for initially imperfect rectangular plates subjected to tent-like temperature distributions. In their study, they incorporated the effects of thermally induced stresses and initial imperfections into von Karman's classical large-deflection theory. Similarly, Forray and Newman (1962) analyzed the postbuckling response of isotropic and rectangular plates heated symmetrically about two orthogonal centerlines. Their formulation provided flexibility in the choice of boundary conditions. Later, using the Rayleigh–Ritz and Galerkin procedures, Mahayni (1966) extended the formulation to the analysis of shallow cylindrical shells subjected to axially parabolic temperature distributions.

Also, Basuli (1968) presented an approach for the large-deflection analysis of plates under stationary temperature distributions based on the concept of total potential energy. In this approach, the energy contribution due to the second invariant of the resultant strains is neglected in the total potential energy expression. This approximation, originally introduced by Berger (1955) for the large-deflection analysis of plates, simplifies the von Karman type of coupled nonlinear partial differential equations to a set of quasi-linear, decoupled equations. Among the few investigations where a Berger–Basuli type of approximation was employed, Pal (1969, 1973) analyzed the static and dynamic instability of heated circular plates subjected to non-uniform temperature distribution both across the surface and through the thickness. For dynamic analysis, Pal (1973) used Hamilton's variational principle to derive the dynamic equilibrium equations of orthotropic plates. In this analysis, it was observed that the bifurcation buckling behavior gradually disappears as the temperature gradients through the thickness increase. Biswas (1974, 1976) considered the quasi-static large deflections of circular plates and equilateral plates under stationary and non-stationary temperature distributions. He provided analytical solutions for circular and equilateral plates by utilizing the Bessel functions and Fourier series expansion, respectively. Biswas (1978, 1981) also presented formulations and solution procedures to analyze the nonlinear behavior of heated orthotropic rectangular plates. He provided a one-term Fourier series approximation for the transverse deflection (Biswas, 1981) by applying Galerkin's approach for the solution of governing equations. This solution method led to a cubic expression relating applied temperature to central transverse deflection.

Unlike the aforementioned approaches for the nonlinear analysis of panels subjected to heating, Huang and Tauchert (1988a, 1988b) directly utilized the total potential energy expression in order to determine the pre- and postbuckling equilibrium configurations of antisymmetric angle-ply laminates subjected to uniform and nonuniform temperature loadings. The minimization of the total potential energy expression is accomplished by the method of conjugate directions (Powell, 1964). With this method, the minimum of a function with respect to several unknown variables is computed without requiring the derivatives of the function with respect to these variables. In order to ensure that the conjugate directions method converges to the actual equilibrium configuration, Huang and Tauchert used an incremental thermal loading procedure.

In order to analyze the thermal postbuckling response of panels with orthotropic material properties,

Raju and Rao (1989) developed a solution based on the Rayleigh–Ritz procedure with a one-term double-sinusoidal admissible function. They provided analytical expressions describing the temperature–displacement path in the postbuckling range. Recently, by using these approximate techniques, Meyers and Hyer (1990, 1991) and Singh et al. (1993) extended the range of this type of analysis to include the nonlinear thermoelastic response of anisotropic panels. Meyers and Hyer utilized the first and second variations of the total potential energy expression to investigate bifurcation and postbuckling responses of quasi-isotropic panels.

Although a majority of the analytical investigations were focused on the energy and variational principles and utilized the total potential energy expression for the derivation of the equations of equilibrium, only a few directly invoked the equations of nonlinear plate theory. In this context, Stavsky (1963) employed the modified compatibility relation and moment equilibrium equations to derive the large-deflection equations for a flat rectangular heterogeneous plate under thermal loading. Librescu and Souza (1991a, 1991b) developed a von Karman type of the large-deflection theory for plates made of transversely isotropic materials under combined uniform temperature rise and in-plane edge loads. Their formulation includes the effects of transverse shear deformations. They focused particular attention on understanding the effects of shear deformations and in-plane edge boundary conditions on the load-carrying capacity of the panel in pre- and postbuckling equilibrium stages. Librescu and Souza (1993) and Librescu et al. (1994, 1995) further extended the nonlinear theory to include the effects of non-uniform temperature distribution on flat and curved panels under combined loading. Across the thickness, the temperature distribution is assumed to vary linearly, with the inner surface of the panel being held at room temperature. Birman and Bert (1993) also considered a combined thermal–mechanical loading. They developed analytic formulations describing the pre- and post-equilibrium paths of shells under thermal loading. Using the analytically derived expressions for the temperature versus central displacement, they identified the snap-through conditions for shells.

Although there has been considerable progress in the analytical predictions of flat and curved panels subjected to thermo-mechanical loading, the range of applicability of these methods is limited to simple panel configurations. In fact, they suffer from generality when applied to structures with complex geometry and boundary conditions. In the context of nonlinear thermo-mechanical analysis of structures by finite element methods, early attempts were reported by Rao and Raju (1984), and Raju and Rao (1984a, 1984b). They obtained solutions for the thermal postbuckling responses of straight (Raju and Rao, 1984a) and tapered (Raju and Rao, 1984b) beams. Based on the approach introduced by Rao and Raju (1984), Chen and Chen (1989, 1991) studied the thermal postbuckling response of laminated plates with and without temperature-dependent material properties.

Madenci and Barut (1994) considered the stability and large deflection of flat and curved composite panels with cutouts subjected to uniform temperatures. This work was extended by Noor and Kim (1996), and Noor and Peters (1996) to the case of thermal postbuckling of laminated panels with cutouts subjected to combined temperature and in-plane compressive and shear loading.

Although methods for large-deflection and stability analysis of flat and curved panels under uniform thermal loading are well established, finite element analyses of postbuckling behavior of composite panels subjected to non-uniform thermal loading are rather few (Noor and Peters, 1997). This study is, therefore, concerned with the finite element formulation of laminates subjected to non-uniform thermal loading both through-the-thickness and over the surface of panels. A detailed analysis of the effect of non-uniform thermal loading on the stability of flat and curved laminates with and without a central hole is presented.

2. Element development

Consider the motion of a shallow triangular shell element at initial ($t = 0$), deformed ($t = t$), and next deformed ($t = t + \Delta t$) configurations as illustrated in Fig. 1. The element dimensions are defined by the thickness (H), area (A), and height ($h(x, y)$), of the element mid-plane with respect to the element reference plane. The non-uniform temperature distribution in the shell element is denoted by $T(x, y, z)$. Based on the co-rotational form of the total Lagrangian formulation, the initial configuration of the shell element, which translates and rotates as the shell element deforms, is utilized in order to express the equilibrium of the shell element.

The formulation begins with the principle of virtual work:

$$\delta \mathscr{W}^{e} = \int_{{}^{0}V} \delta_{0}\boldsymbol{\epsilon}^{T}\, {}^{t+\Delta t}_{0}\mathbf{s}\, \mathrm{d}\, {}^{0}V. \tag{1}$$

Between time t and $t + \Delta t$, ${}_{0}\boldsymbol{\epsilon}$ represents the incremental Green strain tensor in vector form. The components of the Piola–Kirchhoff stress tensor are contained in a vector denoted by ${}^{t+\Delta t}_{0}\mathbf{s}$. The lower-

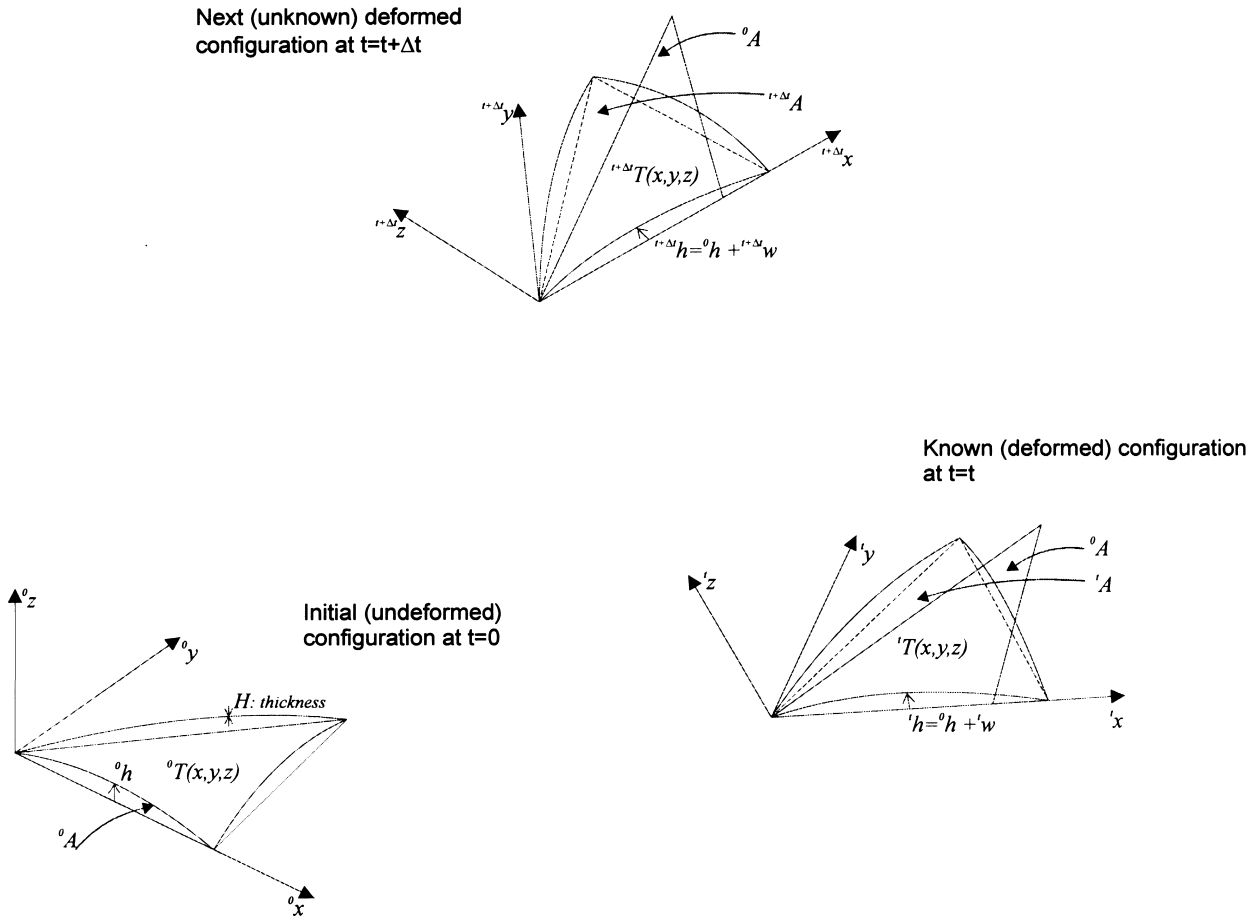

Fig. 1. Motion of a shallow triangular shell element.

left subscript indicates the configuration by which the quantity is measured. The upper-left superscripts refer to the configuration of the body at a specific time. The volume of the element at the initial configuration is denoted by ${}^0V$, and $\delta\mathscr{W}^{\mathrm{e}}$ is the virtual work done by the external forces at time $t+\Delta t$.

Under the assumption that the material properties are temperature independent and remain constant throughout deformation, the Duhamel–Neumann stress–strain relation for an orthotropic material is expressed as

$$ {}^{t+\Delta t}_{0}\mathbf{s} = \mathbf{Q}\left({}^{t+\Delta t}_{0}\boldsymbol{\epsilon} - \boldsymbol{\alpha}\, {}^{t+\Delta t}T\right) = \mathbf{Q}\, {}^{t+\Delta t}_{0}\boldsymbol{\epsilon} - \mathbf{Q}\boldsymbol{\alpha}\, {}^{t+\Delta t}T, \tag{2} $$

in which $\mathbf{Q}$ represents the anisoparametric material properties and $\boldsymbol{\alpha}$ is the vector containing the coefficients of thermal expansion. In Eq. (2), the Green strain tensor in vector form is denoted by ${}^{t+\Delta t}_{0}\boldsymbol{\epsilon}$. The temperature field at time $t+\Delta t$ is represented by ${}^{t+\Delta t}T$. Defining ${}^{t+\Delta t}_{0}\boldsymbol{\sigma}$ and ${}^{t+\Delta t}_{0}\boldsymbol{\tau}$ as

$$ {}^{t+\Delta t}_{0}\boldsymbol{\sigma} = \mathbf{Q}\, {}^{t+\Delta t}_{0}\boldsymbol{\epsilon}, \tag{3a} $$

$$ {}^{t+\Delta t}_{0}\boldsymbol{\tau} = \mathbf{Q}\boldsymbol{\alpha}\, {}^{t+\Delta t}T \tag{3b} $$

and substituting in Eq. (2) yields

$$ {}^{t+\Delta t}_{0}\mathbf{s} = {}^{t+\Delta t}_{0}\boldsymbol{\sigma} - {}^{t+\Delta t}_{0}\boldsymbol{\tau}, \tag{4} $$

where ${}^{t+\Delta t}_{0}\boldsymbol{\sigma}$ and ${}^{t+\Delta t}_{0}\boldsymbol{\tau}$ may be regarded as the Hookean and thermal stress vectors (Nowinski, 1978). Although they do not represent the stresses arising from mechanical and thermal loadings, respectively, their superposition results in the actual (Piola–Kirchhoff) stress vector, ${}^{t+\Delta t}_{0}\mathbf{s}$. Since the strain vector, ${}^{t+\Delta t}_{0}\boldsymbol{\epsilon}$ and the temperature field, ${}^{t+\Delta t}T$, can be decomposed between the time increments, the stress vectors ${}^{t+\Delta t}_{0}\boldsymbol{\sigma}$ and ${}^{t+\Delta t}_{0}\boldsymbol{\tau}$ defined by Eqs. (3a) and (3b) can also be decomposed in time. Thus, the Hookean stress vector ${}^{t+\Delta t}_{0}\boldsymbol{\sigma}$ is decomposed as

$$ {}^{t+\Delta t}_{0}\boldsymbol{\sigma} = {}^{t}_{0}\boldsymbol{\sigma} + {}_{0}\boldsymbol{\sigma}, \tag{5} $$

in which ${}^{t}_{0}\boldsymbol{\sigma}$ and ${}_{0}\boldsymbol{\sigma}$ denote the Hookean stress vectors at time t and in incremental form, respectively. Combining Eqs. (4) and (5) gives

$$ {}^{t+\Delta t}_{0}\mathbf{s} = {}^{t}_{0}\boldsymbol{\sigma} + {}_{0}\boldsymbol{\sigma} - {}^{t+\Delta t}_{0}\boldsymbol{\tau}. \tag{6} $$

Substitution of Eq. (6) for ${}^{t+\Delta t}_{0}\mathbf{s}$ in Eq. (1) results in

$$ \delta\mathscr{W}^{\mathrm{e}} = \int_{{}^0V} \delta_0\boldsymbol{\epsilon}^T\left({}^{t}_{0}\boldsymbol{\sigma} - {}^{t+\Delta t}_{0}\boldsymbol{\tau}\right) \mathrm{d}\, {}^0V + \int_{{}^0V} \delta_0\boldsymbol{\epsilon}^T\, {}_0\boldsymbol{\sigma}\, \mathrm{d}\, {}^0V. \tag{7} $$

The vector of incremental Green strains in Eq. (7) is defined as

$$ \delta_0\boldsymbol{\epsilon} = \delta_0\boldsymbol{\epsilon}_{\mathrm{L}} + \delta_0\boldsymbol{\epsilon}_{\mathrm{N}}, \tag{8} $$

where ${}_0\boldsymbol{\epsilon}_{\mathrm{L}}$ and ${}_0\boldsymbol{\epsilon}_{\mathrm{N}}$ represent the linear and nonlinear parts of the incremental Green strains in vector form, respectively. Also, the incremental Hookean stress vector, ${}_0\boldsymbol{\sigma}$ in Eq. (7), is related to its counterpart, ${}_0\boldsymbol{\epsilon}$, as

$$ {}_0\boldsymbol{\sigma} = \mathbf{Q}\, {}_0\boldsymbol{\epsilon}. \tag{9} $$

Substituting from Eqs. (8) and (9) for the virtual incremental strain and incremental stress components in Eq. (7) and rearranging the terms leads to

$$\delta\mathscr{W}^{e} = \int_{{}^{0}V} \delta_0\boldsymbol{\epsilon}^T \mathbf{Q}\, {}_0\boldsymbol{\epsilon}\, \mathrm{d}\, {}^{0}V + \int_{{}^{0}V} \delta_0\boldsymbol{\epsilon}_{\mathrm{N}}^T\, {}^{t}_{0}\boldsymbol{\sigma}\, \mathrm{d}\, {}^{0}V - \int_{{}^{0}V} \delta_0\boldsymbol{\epsilon}_{\mathrm{N}}^T\, {}^{t+\Delta t}_{0}\boldsymbol{\tau}\, \mathrm{d}\, {}^{0}V + \int_{{}^{0}V} \delta_0\boldsymbol{\epsilon}_{L}^T\, {}^{t}_{0}\boldsymbol{\sigma}\, \mathrm{d}\, {}^{0}V - \int_{{}^{0}V} \delta_0\boldsymbol{\epsilon}_{\mathrm{L}}^T\, {}^{t+\Delta t}_{0}\boldsymbol{\tau}\, \mathrm{d}\, {}^{0}V.$$

The first integral term on the right-hand side of Eq. (10) is nonlinear in terms of incremental displacement components whereas the remaining terms are either linearly related to or independent from the incremental displacement components. The nonlinearity of the first integral term, however, may cause difficulties in the solution of equilibrium equations. In order to relieve such difficulty in the solution process, the linearization procedure outlined by Bathe (1982) can be employed for the evaluation of the first integral term, as the true equilibrium configurations will be searched by an incremental-iterative strategy. Thus, the following approximations are employed:

$$\delta_0\boldsymbol{\epsilon} \cong \delta_0\boldsymbol{\epsilon}_{\mathrm{L}}$$

and

$$\mathbf{Q}\, {}_0\boldsymbol{\epsilon} \cong \mathbf{Q}\, {}_0\boldsymbol{\epsilon}_{\mathrm{L}}. \tag{11}$$

Incorporating Eq. (11) into the first integral term of Eq. (10) and rearranging the terms yields

$$\begin{aligned} &\int_{{}^{0}V} \delta_0\boldsymbol{\epsilon}_{\mathrm{L}}^T \mathbf{Q}\, {}_0\boldsymbol{\epsilon}_{\mathrm{L}}\, \mathrm{d}\, {}^{0}V + \int_{{}^{0}V} \delta_0\boldsymbol{\epsilon}_{\mathrm{N}}^T\, {}^{t}_{0}\boldsymbol{\sigma}\, \mathrm{d}\, {}^{0}V - \int_{{}^{0}V} \delta_0\boldsymbol{\epsilon}_{\mathrm{N}}^T\, {}^{t+\Delta t}_{0}\boldsymbol{\tau}\, \mathrm{d}\, {}^{0}V \\ &\quad = \delta\mathscr{W}^{e} - \int_{{}^{0}V} \delta_0\boldsymbol{\epsilon}_{\mathrm{L}}^T\, {}^{t}_{0}\boldsymbol{\sigma}\, \mathrm{d}\, {}^{0}V + \int_{{}^{0}V} \delta_0\boldsymbol{\epsilon}_{\mathrm{L}}^T\, {}^{t+\Delta t}_{0}\boldsymbol{\tau}\, \mathrm{d}\, {}^{0}V. \end{aligned} \tag{12}$$

As shown in Fig. 2, the element is made of a layered composite laminate. Each layer is assumed to be homogeneous, elastic, and orthotropic with elastic moduli, E_1 and E_2; shear modulus, G_{12}; Poisson's ratio, ν_{12}; and coefficients of thermal expansion, α_1 and α_2. The subscripts '1' and '2' specify the longitudinal and transverse directions relative to the fibers in the layer. Also, the position of each ply with respect to the element mid-plane is denoted by the local coordinate $\bar{z}$. Application of these geometric and layered material properties of the shell element to Eq. (12) yields

$$\begin{aligned} &\sum_{k=1}^{K} \int_{{}^{0}A} \int_{\bar{z}_{k-1}}^{\bar{z}_k} \delta_0\boldsymbol{\epsilon}_{\mathrm{L}}^T \mathbf{Q}^{(k)}\, {}_0\boldsymbol{\epsilon}_{\mathrm{L}}\, d\bar{z}\, \mathrm{d}\, {}^{0}A + \sum_{k=1}^{K} \int_{{}^{0}A} \int_{\bar{z}_{k-1}}^{\bar{z}_k} \delta_0\boldsymbol{\epsilon}_{\mathrm{N}}^T\, {}^{t}_{0}\boldsymbol{\sigma}\, d\bar{z}\, \mathrm{d}\, {}^{0}A - \int_{{}^{0}A} \int_{\bar{z}_{k-1}}^{\bar{z}_k} \delta_0\boldsymbol{\epsilon}_{\mathrm{N}}^T\, {}^{t+\Delta t}_{0}\boldsymbol{\tau}\, d\bar{z}\, \mathrm{d}\, {}^{0}A \\ &\quad = \delta\mathscr{W}^{e} - \sum_{k=1}^{K} \int_{{}^{0}A} \int_{\bar{z}_{k-1}}^{\bar{z}_k} \delta_0\boldsymbol{\epsilon}_{\mathrm{L}}^T\, {}^{t}_{0}\boldsymbol{\sigma}\, d\bar{z}\, \mathrm{d}\, {}^{0}A + \sum_{k=1}^{K} \int_{{}^{0}A} \int_{\bar{z}_{k-1}}^{\bar{z}_k} \delta_0\boldsymbol{\epsilon}_{\mathrm{L}}^T\, {}^{t+\Delta t}_{0}\boldsymbol{\tau}\, d\bar{z}\, \mathrm{d}\, {}^{0}A, \end{aligned}$$

where K denotes the number of plies forming the laminate. The thickness of the k^{th} layer is given by $t_k = \bar{z}_k - \bar{z}_{k-1}$. Material property matrix $\bar{\mathbf{Q}}^{(k)}$ designates the k^{th} orthotropic lamina and is referenced to the $(x$–$y)$ element coordinate system, as shown in Fig. 2.

2.1. Displacement field

In accordance with Mindlin's theory (Mindlin, 1951), the incremental displacement components u, v, and w in the x, y, and $\bar{z}$ directions are expressed as

$$u(x, y, \bar{z}) = u_0(x, y) + \bar{z}\theta_y(x, y),$$

$$v(x, y, \bar{z}) = v_0(x, y) + \bar{z}\theta_x(x, y)$$

and

$$w(x, y, \bar{z}) = w_0(x, y). \tag{14}$$

The functions u_0 and v_0 represent the in-plane displacements and w_0 the out-of-plane displacements on the mid-surface of the element. The bending (normal) rotations about the x- and y-axes are denoted by θ_x and θ_y, respectively. The element coordinate system is chosen such that the positive x-axis points in the direction from node 1 to node 2 of the element. As shown in Fig. 2, the element reference plane coincides with the (x–y) plane. The components of the incremental displacements and bending rotations

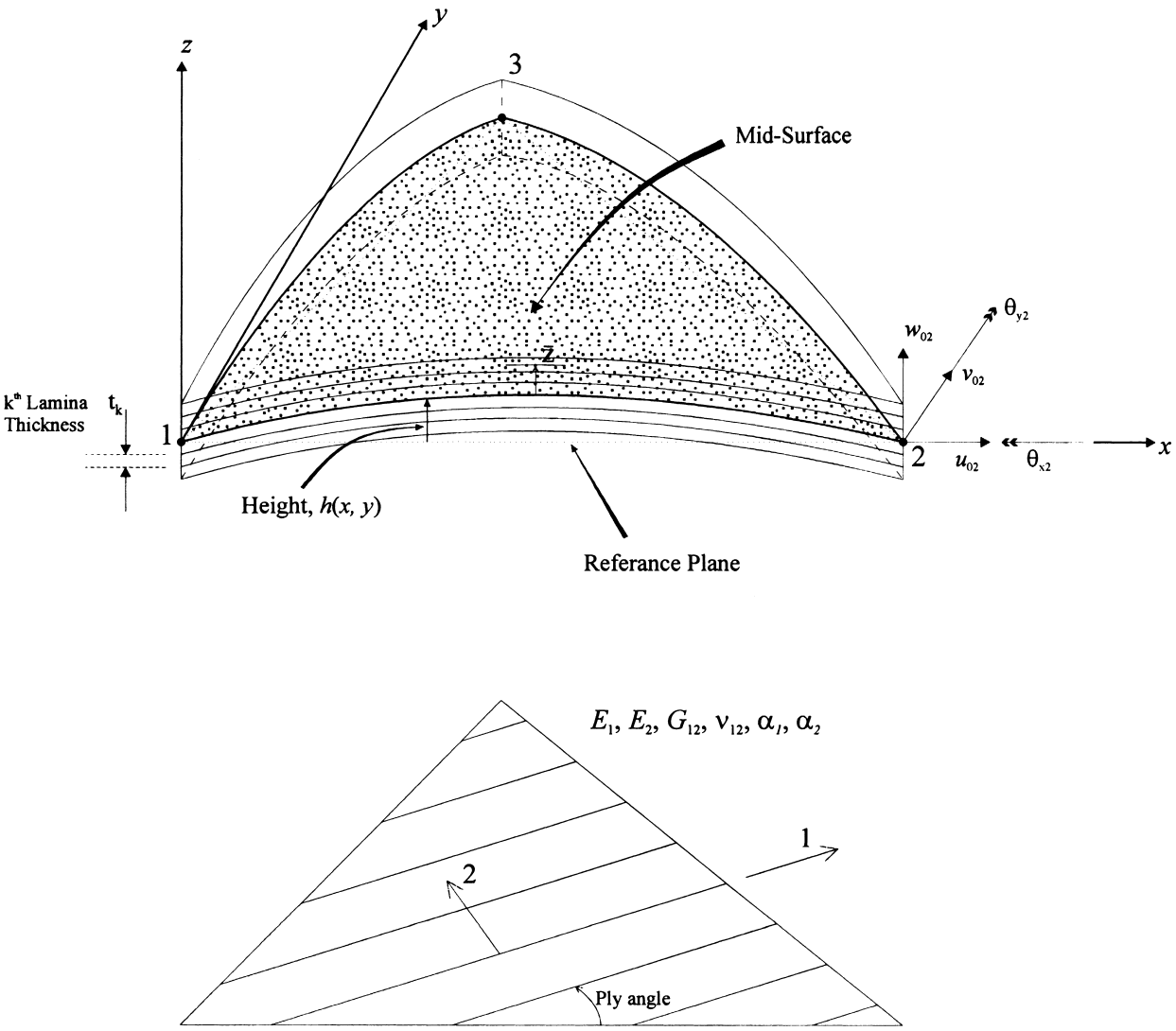

Fig. 2. Geometry and material layout of the shallow shell element with the positive directions of nodal displacements and rotations.

at each node of the element, with positive sign conventions, are illustrated in Fig. 2. The variable $\bar{z}$ is defined as

$$\bar{z} = z - h(x, y), \tag{15}$$

where $h(x, y)$ describes the shallow mid-surface of the shell element.

2.2. Strain field

The linear part of the Green's strain tensor is based on the definitions given by Reissner (1945) and Mindlin (1951), combined with the shallow shell theory introduced by Marguerre (1938). The nonlinear strain vector, ${}_0\boldsymbol{\epsilon}_{\mathrm{N}}$, is the von Karman (1910) approximation of its complete form (i.e., the nonlinear terms due to the gradients of in-plane mid-surface displacements are also included). Therefore, the linear and nonlinear parts of the incremental Green's strain tensor for the shallow shell component are defined as

$${}_0\boldsymbol{\epsilon}_{\mathrm{L}} = \begin{Bmatrix} u_{0,x} - {}^t h_{,x}\theta_y \\ v_{0,y} - {}^t h_{,y}\theta_x \\ u_{0,y} + v_{0,x} - {}^t h_{,x}\theta_x - {}^t h_{,y}\theta_y \\ w_{0,x} + \theta_y \\ w_{0,y} + \theta_x \end{Bmatrix} + \bar{z}\begin{Bmatrix} \theta_{y,x} \\ \theta_{x,y} \\ \theta_{x,x} + \theta_{y,y} \\ 0 \\ 0 \end{Bmatrix} \tag{16a}$$

and

$${}_0\boldsymbol{\epsilon}_{\mathrm{N}} = \frac{1}{2}\begin{Bmatrix} u_{0,x}^2 + v_{0,x}^2 + w_{0,x}^2 \\ u_{0,y}^2 + v_{0,y}^2 + w_{0,y}^2 \\ 2(u_{0,x}u_{0,y} + v_{0,x}v_{0,y} + w_{0,x}w_{0,y}) \\ 0 \\ 0 \end{Bmatrix}. \tag{16b}$$

Substituting Eqs. (16a) and (16b) for the incremental strain components and performing integration along the thickness direction in Eq. (13) leads to

$$\begin{aligned} &\int_{{}^0A} \delta_0\mathbf{e}_{\mathrm{L}}^T \mathbf{C}\, {}_0\mathbf{e}_{\mathrm{L}}\, \mathrm{d}\, {}^0A + \int_{{}^0A} \delta_0\mathbf{e}_{\mathrm{N}}^T\, {}_0^t\hat{\boldsymbol{\sigma}}\, \mathrm{d}\, {}^0A - \int_{{}^0A} \delta_0\mathbf{e}_{\mathrm{N}}^T\, {}_0^{t+\Delta t}\hat{\boldsymbol{\tau}}\, \mathrm{d}\, {}^0A \\ &\quad = \delta\mathscr{W}^{\mathrm{e}} - \int_{{}^0A} \delta_0\mathbf{e}_{\mathrm{L}}^T\, {}_0^t\hat{\boldsymbol{\sigma}}\, \mathrm{d}\, {}^0A + \int_{{}^0A} \delta_0\mathbf{e}_{\mathrm{L}}^T\, {}_0^{t+\Delta t}\hat{\boldsymbol{\tau}}\, \mathrm{d}\, {}^0A, \end{aligned} \tag{17}$$

in which $\mathbf{C}$ is the constitutive matrix composed of the extensional, $\mathbf{A}$, membrane-bending coupling, $\mathbf{B}$, bending, $\mathbf{D}$ and transverse shear, $\mathbf{G}$, stiffness matrices (Yang et al., 1966),

$$\mathbf{C} = \begin{bmatrix} \mathbf{A} & \mathbf{B} & \mathbf{0} \\ \mathbf{B} & \mathbf{D} & \mathbf{0} \\ \mathbf{0} & \mathbf{0} & \mathbf{G} \end{bmatrix}, \tag{18}$$

with

$$\left.\begin{aligned} A_{ij} &= \sum_{k=1}^{K} Q_{ij}^{(k)}(\bar{z}_k - \bar{z}_{k-1}) \\ B_{ij} &= \frac{1}{2}\sum_{k=1}^{K} Q_{ij}^{(k)}\left(\bar{z}_k^2 - \bar{z}_{k-1}^2\right) \\ D_{ij} &= \frac{1}{3}\sum_{k=1}^{K} Q_{ij}^{(n)}\left(\bar{z}_k^3 - \bar{z}_{k-1}^3\right) \\ G_{lm} &= \sum_{k=1}^{K} Q_{l+3,\,m+3}^{(n)}(\bar{z}_k - \bar{z}_{k-1}) \end{aligned}\right\} \begin{matrix} i,j = 1,2,3 \\ l,m = 1,2 \end{matrix}. \tag{19}$$

The vectors ${}^{t}_{0}\hat{\boldsymbol{\sigma}}$ and ${}^{t+\Delta t}_{0}\hat{\boldsymbol{\tau}}$ contain, respectively, the following stress resultants:

$${}^{t}_{0}\hat{\boldsymbol{\sigma}}^{T} = \left\{ {}^{t}_{0}\hat{\boldsymbol{\sigma}}_{\epsilon}^{T},\ {}^{t}_{0}\hat{\boldsymbol{\sigma}}_{\kappa}^{T},\ {}^{t}_{0}\hat{\boldsymbol{\sigma}}_{\gamma}^{T} \right\} \tag{20a}$$

and

$${}^{t+\Delta t}_{0}\hat{\boldsymbol{\tau}}^{T} = \left\{ {}^{t+\Delta t}_{0}\hat{\boldsymbol{\tau}}_{\epsilon}^{T},\ {}^{t+\Delta t}_{0}\hat{\boldsymbol{\tau}}_{\kappa}^{T},\ {}^{t+\Delta t}_{0}\hat{\boldsymbol{\tau}}_{\gamma}^{T} \right\}, \tag{20b}$$

where the subscripts ϵ, κ and γ denote the Hookean and thermal stress resultants associated with the in-plane, bending and transverse shear deformations, respectively. These stress resultant vectors are established by integrating the Hookean (${}^{t}_{0}\boldsymbol{\sigma}$) and the thermal stress (${}^{t+\Delta t}_{0}\boldsymbol{\tau}$) vectors across the thickness of the panel as given by

$$\left({}^{t}_{0}\hat{\boldsymbol{\sigma}}_{\epsilon},\ {}^{t+\Delta t}_{0}\hat{\boldsymbol{\tau}}_{\epsilon}\right) = \left(\begin{Bmatrix} {}^{t}_{0}N_{\sigma xx} \\ {}^{t}_{0}N_{\sigma yy} \\ {}^{t}_{0}N_{\sigma xy} \end{Bmatrix}, \begin{Bmatrix} {}^{t+\Delta t}_{0}N_{\tau xx} \\ {}^{t+\Delta t}_{0}N_{\tau yy} \\ {}^{t+\Delta t}_{0}N_{\tau xy} \end{Bmatrix} \right) = \sum_{k=1}^{K} \int_{\bar{z}_{k-1}}^{\bar{z}_k} \left(\begin{Bmatrix} {}^{t}_{0}\sigma_{xx} \\ {}^{t}_{0}\sigma_{yy} \\ {}^{t}_{0}\sigma_{xy} \end{Bmatrix}, \begin{Bmatrix} {}^{t+\Delta t}_{0}\tau_{xx} \\ {}^{t+\Delta t}_{0}\tau_{yy} \\ {}^{t+\Delta t}_{0}\tau_{xy} \end{Bmatrix} \right) d\bar{z}, \tag{21a}$$

$$\left({}^{t}_{0}\hat{\boldsymbol{\sigma}}_{\kappa},\ {}^{t+\Delta t}_{0}\hat{\boldsymbol{\tau}}_{\kappa}\right) = \left(\begin{Bmatrix} {}^{t}_{0}M_{\sigma xx} \\ {}^{t}_{0}M_{\sigma yy} \\ {}^{t}_{0}M_{\sigma xy} \end{Bmatrix}, \begin{Bmatrix} {}^{t+\Delta t}_{0}M_{\tau xx} \\ {}^{t+\Delta t}_{0}M_{\tau yy} \\ {}^{t+\Delta t}_{0}M_{\tau xy} \end{Bmatrix} \right) = \sum_{k=1}^{K} \int_{\bar{z}_{k-1}}^{\bar{z}_k} z \left(\begin{Bmatrix} {}^{t}_{0}\sigma_{xx} \\ {}^{t}_{0}\sigma_{yy} \\ {}^{t}_{0}\sigma_{xy} \end{Bmatrix}, \begin{Bmatrix} {}^{t+\Delta t}_{0}\tau_{xx} \\ {}^{t+\Delta t}_{0}\tau_{yy} \\ {}^{t+\Delta t}_{0}\tau_{xy} \end{Bmatrix} \right) d\bar{z} \tag{21b}$$

and

$$\left({}^{t}_{0}\hat{\boldsymbol{\sigma}}_{\gamma},\ {}^{t+\Delta t}_{0}\hat{\boldsymbol{\tau}}_{\gamma}\right) = \left(\begin{Bmatrix} {}^{t}_{0}Q_{\sigma xz} \\ {}^{t}_{0}Q_{\sigma yz} \end{Bmatrix}, \begin{Bmatrix} {}^{t+\Delta t}_{0}Q_{\tau xz} \\ {}^{t+\Delta t}_{0}Q_{\tau yz} \end{Bmatrix} \right) = \sum_{k=1}^{K} \int_{\bar{z}_{k-1}}^{\bar{z}_k} \left(\begin{Bmatrix} {}^{t}_{0}\sigma_{xz} \\ {}^{t}_{0}\sigma_{yz} \end{Bmatrix}, \begin{Bmatrix} {}^{t+\Delta t}_{0}\tau_{xz} \\ {}^{t+\Delta t}_{0}\tau_{yz} \end{Bmatrix} \right) d\bar{z}. \tag{21c}$$

The vectors ${}_{0}\mathbf{e}_{\mathrm{L}}$ and ${}_{0}\mathbf{e}_{\mathrm{N}}$, containing, respectively, the linear and nonlinear parts of the Green strain components measured at the mid-surface, are defined as

$${}_{0}\mathbf{e}_{\mathrm{L}}^{T} = \left\{ {}_{0}\mathbf{e}_{\epsilon\mathrm{L}}^{T},\ {}_{0}\mathbf{e}_{\kappa\mathrm{L}}^{T},\ {}_{0}\mathbf{e}_{\gamma\mathrm{L}}^{T} \right\}, \tag{22}$$

with

$$ {}_0\mathbf{e}_{\epsilon \mathrm{L}} = \left\{ \begin{array}{l} u_{0,x} - {}^t h_{,x}\theta_y \\ v_{0,y} - {}^t h_{,y}\theta_x \\ u_{0,y} + v_{0,x} - {}^t h_{,x}\theta_x - {}^t h_{,y}\theta_y \end{array} \right\}, \tag{23a} $$

$$ {}_0\mathbf{e}_{\kappa \mathrm{L}} = \left\{ \begin{array}{l} \theta_{y,x} \\ \theta_{x,y} \\ \theta_{x,x} + \theta_{y,y} \end{array} \right\}, \tag{23b} $$

$$ {}_0\mathbf{e}_{\gamma \mathrm{L}} = \left\{ \begin{array}{l} w_{0,x} + \theta_y \\ w_{0,y} + \theta_x \end{array} \right\} \tag{23c} $$

and

$$ {}_0\mathbf{e}_{\mathrm{N}} = \left\{ {}_0\mathbf{e}_{\epsilon \mathrm{N}}^T, \mathbf{0}^T, \mathbf{0}^T \right\}, \tag{24} $$

with

$$ {}_0\mathbf{e}_{\epsilon \mathrm{N}} = \frac{1}{2} \left\{ \begin{array}{l} u_{0,x}^2 + v_{0,x}^2 + w_{0,x}^2 \\ u_{0,y}^2 + v_{0,y}^2 + w_{0,y}^2 \\ 2(u_{0,x}u_{0,y} + v_{0,x}v_{0,y} + w_{0,x}w_{0,y}) \end{array} \right\}. \tag{25} $$

Utilizing the C^0-anisoparametric interpolation functions derived by Tessler (1990), the incremental in-plane, transverse, and out-of-plane rotational components on the mid-surface of the element are approximated as

$$ \left\{ \begin{array}{l} u_0 \\ v_0 \end{array} \right\} = \sum_{k=1}^{3} \mathscr{N}_k \left\{ \begin{array}{l} u_{0k} \\ v_{0k} \end{array} \right\} + \sum_{k=4}^{9} \mathscr{N}_k \left\{ \begin{array}{l} u_{0k}^+ \\ v_{0k}^+ \end{array} \right\} + \mathscr{N}_c \left\{ \begin{array}{l} u_{0c} \\ v_{0c} \end{array} \right\}, $$

$$ w_0 = \sum_{k=1}^{3} \mathscr{M}_k w_{0k} + \sum_{k=4}^{6} \mathscr{M}_k w_{0k}^+ $$

and

$$ \left\{ \begin{array}{l} \theta_x \\ \theta_y \end{array} \right\} = \sum_{k=1}^{3} \zeta_k \left\{ \begin{array}{l} \theta_{xk} \\ \theta_{yk} \end{array} \right\}. \tag{26} $$

The in-plane displacement components, u_0 and v_0, are approximated by cubic interpolation functions, $\mathscr{N}_k$ and $\mathscr{N}_c$. The nodal values at the vertices are represented by u_{0k} and v_{0k}. The remaining nodal values are associated with the nodes along the edges, u_{0k}^+ and v_{0k}^+, and at the element centroid, u_{0c} and v_{0c}. The transverse displacement field, w_0, is approximated by quadratic interpolation functions, $\mathscr{M}_k$, with w_{0k} and w_{0k}^+ representing the nodal values at the vertices and the middle of the edges, respectively. The out-of-plane rotational components, θ_x and θ_y, are approximated by linear interpolation functions, ζ_k, with θ_{xk} and θ_{yk} representing nodal values at the vertices. The explicit forms of these interpolation functions are given in Appendix A.

In matrix form, Eq. (26) can be rewritten as

$$\mathbf{u}_0 = \mathbf{N}_u\mathbf{v} + \overset{+}{\mathbf{N}}\overset{+}{\mathbf{v}} + \mathbf{N}_c\mathbf{v}_c \tag{27a}$$

and

$$\boldsymbol{\theta}_0 = \mathbf{N}_\theta\mathbf{v}, \tag{27b}$$

where

$$\mathbf{u}_0^T = \{u_0,\ v_0,\ w_0\} \text{ and } \boldsymbol{\theta}_0^T = \{\theta_x,\ \theta_y,\ 0\},$$

$$\mathbf{v}^T = \{u_{01},\ v_{01},\ w_{01},\ \theta_{x1},\ \theta_{y1},\ \theta_{z1}, \ldots,\ u_{03},\ v_{03},\ w_{03},\ \theta_{x3},\ \theta_{y3},\ \theta_{z3}\},$$

$$\overset{+}{\mathbf{v}}{}^T = \left\{u_{04}^+, \ldots,\ u_{09}^+,\ v_{04}^+, \ldots,\ v_{09}^+,\ w_{04}^+,\ w_{05}^+,\ w_{06}^+\right\}$$

and

$$\mathbf{v}_c^T = \{u_{0c},\ v_{0c}\}.$$

The shape-function matrices $\mathbf{N}_u$ and $\mathbf{N}_u^+$ are dependent on $\mathscr{N}_k$ and $\mathscr{M}_k$, with $k = 1,..., 9$ and $k = 1,..., 6$, respectively. The matrix $\mathbf{N}_c$ contains only $\mathscr{N}_c$. The matrix $\mathbf{N}_\theta$ is composed of the area coordinates ξ_k, with $k = 1, 2, 3$. Although it is artificial, the rotational variable normal to the reference plane, θ_{zk}, is included in the formulation because transformation to global coordinates leads to non-zero rotations about all axes. The explicit expressions for the shape-function matrices are given in Appendix A.

The in-plane and transverse displacement components at the edge nodes are eliminated prior to the construction of the stiffness matrix by imposing the edge constraints on the linear part of the shear membrane strains. These constraints, introduced by Tessler (1990), are given in the form

$$\frac{\partial}{\partial s}\left[\frac{\partial}{\partial s}w_0(s) + \theta_n(s)\right]^{(k)} = 0$$

and

$$\frac{\partial^{\,p}}{\partial s^{\,p}}\begin{Bmatrix} \dfrac{\partial}{\partial s}u_s(s) - \theta_n\dfrac{\partial}{\partial s}h(n,\ s) \\ \dfrac{\partial}{\partial s}v_n(s) - \theta_n\dfrac{\partial}{\partial n}h(n,\ s) - \theta_s\dfrac{\partial}{\partial s}h(n,\ s) \end{Bmatrix} = 0, \tag{28}$$

with $k = 1, 2, 3$ and $p = 1, 2$. The subscripts r and n denote the directions tangent and normal to the edge of the element. The k^{th} edge is specified by a superscript k. The displacement components tangent and normal to the k^{th} edge of the element are denoted by $u(s)$ and $v(s)$, respectively. These displacements and rotations are related to their counterparts, defined with respect to the element coordinates, through appropriate transformations.

Imposing the constraints given by Eq. (28) along the edge of the element leads to the following transformation between intra-edge displacements and corner displacements:

$$\overset{+}{\mathbf{v}}_\beta = \mathbf{L}_\beta\mathbf{v} \text{ with } \beta = u,\ v,\ w \tag{29}$$

or

$$\overset{+}{\mathbf{v}} = \mathbf{L}\mathbf{v}, \tag{30}$$

where

$$\mathbf{L}^T = \left[\mathbf{L}_u^T\ \mathbf{L}_v^T\ \mathbf{L}_w^T\right]$$

and

$$\overset{+}{\mathbf{v}}^T = \begin{bmatrix} \overset{+}{\mathbf{v}}_u^T & \overset{+}{\mathbf{v}}_v^T & \overset{+}{\mathbf{v}}_w^T \end{bmatrix}, \tag{31}$$

with

$$\overset{+}{\mathbf{v}}_u^T = \left\{u_{04}^+, \ldots, u_{09}^+\right\},$$

$$\overset{+}{\mathbf{v}}_v^T = \left\{v_{04}^+, \ldots, v_{09}^+\right\}$$

and

$$\overset{+}{\mathbf{v}}_w^T = \left\{w_{04}^+, w_{05}^+, w_{06}^+\right\}.$$

The explicit forms of the transformation matrices $\mathbf{L}_\beta$ ($\beta = u,\ v,\ w$) are the same as those given by Tessler (1990). These matrices are presented in Appendix A for completeness.

After substitution from Eq. (30) into Eqs. (27a) and (27b) can be expressed in compact form as

$$\begin{Bmatrix} \mathbf{u}_0 \\ \boldsymbol{\theta}_0 \end{Bmatrix} = \begin{bmatrix} \bar{\mathbf{N}}_u & \mathbf{N}_c \\ \mathbf{N}_\theta & \mathbf{0} \end{bmatrix} \begin{Bmatrix} \mathbf{v} \\ \mathbf{v}_c \end{Bmatrix}, \tag{32}$$

in which $\bar{\mathbf{N}}_u = \mathbf{N}_u + \mathbf{N}_u^+\mathbf{L}$. Based on this form, the linear part of the strain vector, ${}_0\mathbf{e}_\mathrm{L}$, given by Eq. (16a) can be cast into

$${}_0\mathbf{e}_\mathrm{L} = [\mathbf{B}_u,\ \mathbf{B}_\theta] \begin{Bmatrix} \mathbf{u}_0 \\ \boldsymbol{\theta}_0 \end{Bmatrix}, \tag{33}$$

where $\mathbf{B}_u$ and $\mathbf{B}_\theta$ constitute the strain–displacement transformation matrices. The explicit forms of $\mathbf{B}_u$ and $\mathbf{B}_\theta$ are given in Appendix A. Considering ${}_0\mathbf{e}_\mathrm{L}$ in Eq. (33), the first integral in Eq. (17) can be expressed in the form

$$\int_{{}^0A} \delta_0\mathbf{e}_\mathrm{L}^T \mathbf{C}\ {}_0\mathbf{e}_\mathrm{L}\ \mathrm{d}\ {}^0A = \begin{Bmatrix} \delta\mathbf{v} \\ \delta\mathbf{v}_c \end{Bmatrix} \begin{bmatrix} \mathbf{k}_{L11} & \mathbf{k}_{L12} \\ \mathbf{k}_{L12}^T & \mathbf{k}_{L22} \end{bmatrix} \begin{Bmatrix} \mathbf{v} \\ \mathbf{v}_c \end{Bmatrix}, \tag{34}$$

in which

$$\mathbf{k}_{L11} = \int_{{}^0A} \left(\bar{\mathbf{N}}_u^T\mathbf{B}_u^T\mathbf{C}\mathbf{B}_u\bar{\mathbf{N}}_u + \bar{\mathbf{N}}_u^T\mathbf{B}_u^T\mathbf{C}\mathbf{B}_\theta\mathbf{N}_\theta + \mathbf{N}_\theta^T\mathbf{B}_\theta^T\mathbf{C}\mathbf{B}_u\bar{\mathbf{N}}_u + \mathbf{N}_\theta^T\mathbf{B}_\theta^T\mathbf{C}\mathbf{B}_\theta\mathbf{N}_\theta\right)\mathrm{d}^0A,$$

$$\mathbf{k}_{L12} = \int_{{}^0A} \left(\tilde{\mathbf{N}}_u^T \mathbf{B}_u^T \mathbf{C} \mathbf{B}_u \mathbf{N}_c + \mathbf{N}_\theta^T \mathbf{B}_\theta^T \mathbf{C} \mathbf{B}_u \mathbf{N}_c \right) \mathrm{d}^0 A$$

and

$$\mathbf{k}_{L22} = \int_{{}^0A} \mathbf{N}_c^T \mathbf{B}_u^T \mathbf{C} \mathbf{B}_u \mathbf{N}_c \, \mathrm{d}^0 A.$$

In matrix form, the nonlinear part of the strain vector, ${}_0\mathbf{e}_\mathrm{N}$, given by Eq. (16b) becomes

$${}_0\mathbf{e}_\mathrm{N}^T = \frac{1}{2}\{\boldsymbol{\varepsilon}^T \mathfrak{D}^T, \mathbf{0}^T, \mathbf{0}^T\}, \tag{35}$$

in which

$$\boldsymbol{\varepsilon} = \{u_{0,x}, v_{0,x}, w_{0,x}, u_{0,y}, v_{0,y}, w_{0,y}\} \tag{36a}$$

and

$$\mathfrak{D} = \begin{bmatrix} u_{0,x} & v_{0,x} & w_{0,x} & 0 & 0 & 0 \\ 0 & 0 & 0 & u_{0,y} & v_{0,y} & w_{0,y} \\ u_{0,y} & v_{0,y} & w_{0,y} & u_{0,x} & v_{0,x} & w_{0,x} \end{bmatrix}, \tag{36b}$$

with the properties of

$$\delta\mathfrak{D}\boldsymbol{\varepsilon} = \mathfrak{D}\delta\boldsymbol{\varepsilon}$$

and

$$\mathfrak{D}^T \left({}^t_0\hat{\boldsymbol{\sigma}}_\epsilon, {}^{t+\Delta t}_0\hat{\boldsymbol{\tau}}_\epsilon \right) = \left({}^t_0\mathfrak{S}_\epsilon, {}^{t+\Delta t}_0\mathfrak{T}_\epsilon \right)\boldsymbol{\varepsilon}, \tag{37}$$

where

$${}^t_0\mathfrak{S}_\epsilon = \begin{bmatrix} {}^t_0N_{\sigma xx}\mathbf{I} & {}^t_0N_{\sigma xy}\mathbf{I} \\ {}^t_0N_{\sigma xy}\mathbf{I} & {}^t_0N_{\sigma yy}\mathbf{I} \end{bmatrix} \tag{38a}$$

and

$${}^{t+\Delta t}_0\mathfrak{T}_\epsilon = \begin{bmatrix} {}^{t+\Delta t}_0N_{\tau xx}\mathbf{I} & {}^{t+\Delta t}_0N_{\tau xy}\mathbf{I} \\ {}^{t+\Delta t}_0N_{\tau xy}\mathbf{I} & {}^{t+\Delta t}_0N_{\tau yy}\mathbf{I} \end{bmatrix}, \tag{38b}$$

with $\mathbf{I}$ being a 3×3 identity matrix. The vector $\mathbf{E}$ can be expressed in the form

$$\boldsymbol{\varepsilon} = \mathfrak{B}\mathbf{u}_0, \tag{39}$$

with the matrix differential operator

$$\mathfrak{B}^T = \left[\mathbf{I}\frac{\partial}{\partial x}, \mathbf{I}\frac{\partial}{\partial y} \right]. \tag{40}$$

Using this representation of ${}_0\mathbf{e}_\mathrm{N}$ and substituting for $\mathbf{u}_0$ from Eq. (32), the second and the third integral terms in Eq. (17) can be rewritten as

$$\int_{{}^0A} \delta_0\mathbf{e}_{\mathrm{N}}^T\, {}^t_0\hat{\boldsymbol{\sigma}}\, \mathrm{d}^0A = \begin{Bmatrix} \delta\mathbf{v} \\ \delta\mathbf{v}_c \end{Bmatrix}^T \begin{bmatrix} \mathbf{k}_{\sigma 11} & \mathbf{k}_{\sigma 12} \\ \mathbf{k}_{\sigma 12}^T & \mathbf{k}_{\sigma 22} \end{bmatrix} \begin{Bmatrix} \mathbf{v} \\ \mathbf{v}_c \end{Bmatrix}, \tag{41a}$$

in which

$$\mathbf{k}_{\sigma 11} = \int_{{}^0A} \bar{\mathbf{N}}_u^T \mathfrak{B}^T\, {}^t_0\mathfrak{S}_\epsilon \mathfrak{B} \bar{\mathbf{N}}_u\, \mathrm{d}^0A,$$

$$\mathbf{k}_{\sigma 12} = \int_{{}^0A} \bar{\mathbf{N}}_u^T \mathfrak{B}^T\, {}^t_0\mathfrak{S}_\epsilon \mathfrak{B} \mathbf{N}_c\, \mathrm{d}^0A,$$

$$\mathbf{k}_{\sigma 22} = \int_{{}^0A} \mathbf{N}_c^T \mathfrak{B}^T\, {}^t_0\mathfrak{S}_\epsilon \mathfrak{B} \mathbf{N}_c\, \mathrm{d}^0A$$

and

$$\int_{{}^0A} \delta_0\mathbf{e}_{\mathrm{N}}^T\, {}^{t+\Delta t}_0\hat{\boldsymbol{\tau}}_\epsilon\, \mathrm{d}^0A = \begin{Bmatrix} \delta\mathbf{v} \\ \delta\mathbf{v}_c \end{Bmatrix}^T \begin{bmatrix} \mathbf{k}_{\tau 11} & \mathbf{k}_{\tau 12} \\ \mathbf{k}_{\tau 12}^T & \mathbf{k}_{\tau 22} \end{bmatrix} \begin{Bmatrix} \mathbf{v} \\ \mathbf{v}_c \end{Bmatrix}, \tag{41b}$$

in which

$$\mathbf{k}_{\tau 11} = \int_{{}^0A} \bar{\mathbf{N}}_u^T \mathfrak{B}^T\, {}^{t+\Delta t}_0\mathfrak{T}_\epsilon \mathfrak{B} \bar{\mathbf{N}}_u\, \mathrm{d}^0A,$$

$$\mathbf{k}_{\tau 12} = \int_{{}^0A} \bar{\mathbf{N}}_u^T \mathfrak{B}^T\, {}^{t+\Delta t}_0\mathfrak{T}_\epsilon \mathfrak{B} \mathbf{N}_c\, \mathrm{d}^0A$$

and

$$\mathbf{k}_{\tau 22} = \int_{{}^0A} \mathbf{N}_c^T \mathfrak{B}^T\, {}^{t+\Delta t}_0\mathfrak{T}_\epsilon \mathfrak{B} \mathbf{N}_c\, \mathrm{d}^0A.$$

Similarly, by using the incremental linear strain–displacement relations from Eq. (33) and the finite element displacement approximations given by Eq. (32), the fourth and the fifth integral terms in Eq. (17) can be expressed in the following form:

$$\int_{{}^0A} \delta_0\mathbf{e}_{\mathrm{L}}^T\, {}^t_0\hat{\boldsymbol{\sigma}}\, \mathrm{d}^0A = \begin{Bmatrix} \delta\mathbf{v} \\ \delta\mathbf{v}_c \end{Bmatrix}^T \begin{Bmatrix} \mathbf{f}_\sigma \\ \mathbf{f}_{\sigma c} \end{Bmatrix}, \tag{42}$$

in which

$$\mathbf{f}_\sigma = \int_{{}^0A} \left(\bar{\mathbf{N}}_u^T \mathbf{B}_u^T + \mathbf{N}_\theta^T \mathbf{B}_\theta^T \right) {}^t_0\hat{\boldsymbol{\sigma}}\, \mathrm{d}^0A, \tag{43a}$$

$$\mathbf{f}_{\sigma c} = \int_{{}^0A} \mathbf{N}_c^T \mathbf{B}_c^T\, {}^t_0\hat{\boldsymbol{\sigma}}\, \mathrm{d}^0A \tag{43b}$$

and

$$\int_{{}_0A} \delta_0\mathbf{e}_{\mathrm{L}}^T \, {}_0^{t+\Delta t}\hat{\boldsymbol{\tau}} \, \mathrm{d}^0A = \begin{Bmatrix} \delta\mathbf{v} \\ \delta\mathbf{v}_c \end{Bmatrix}^T \begin{Bmatrix} \mathbf{f}_\tau \\ \mathbf{f}_{\tau c} \end{Bmatrix}, \tag{44}$$

in which

$$\mathbf{f}_\tau = \int_{{}_0A} \left(\bar{\mathbf{N}}_u^T \mathbf{B}_u^T + \mathbf{N}_\theta^T \mathbf{B}_\theta^T \right) {}_0^{t+\Delta t}\hat{\boldsymbol{\tau}} \, \mathrm{d}^0A \tag{45a}$$

and

$$\mathbf{f}_{\tau c} = \int_{{}_0A} \mathbf{N}_c^T \mathbf{B}_c^T \, {}_0^{t+\Delta t}\hat{\boldsymbol{\tau}} \, \mathrm{d}^0A \tag{45b}$$

2.3. Computation of internal forces

In order to complete the finite element formulation of the geometric stiffness matrices, $\mathbf{k}_{\sigma ij}$ and $\mathbf{k}_{\tau ij}$, and internal force vectors, ($\mathbf{f}_\sigma$, $\mathbf{f}_{\sigma c}$) and ($\mathbf{f}_\tau$, $\mathbf{f}_{\tau c}$), the resultant stress vectors ${}_0^t\hat{\boldsymbol{\sigma}}$ and ${}_0^{t+\Delta t}\hat{\boldsymbol{\tau}}$ must be determined a priori. The resultant stress vector ${}_0^t\boldsymbol{\sigma}$ can be determined incrementally based on the stress decomposition expressed as

$${}_0^t\hat{\boldsymbol{\sigma}} = {}_0^{t-\Delta t}\hat{\boldsymbol{\sigma}} + {}_0\hat{\boldsymbol{\sigma}}^*, \tag{46}$$

where ${}_0\hat{\boldsymbol{\sigma}}^*$ represents the incremental resultant stress vector (Hookean) in the preceding time step. The vector ${}_0\hat{\boldsymbol{\sigma}}^*$ is related to the incremental resultant strain vector, ${}_0\mathbf{e}^*$, in the preceding time step, by the constitutive relation

$${}_0\hat{\boldsymbol{\sigma}}^* = \mathbf{C} \, {}_0\mathbf{e}^*. \tag{47}$$

The incremental resultant strain vector, ${}_0\mathbf{e}^*$, is composed of its linear and nonlinear components in the form

$${}_0\mathbf{e}^* = {}_0\mathbf{e}_{\mathrm{L}}^* + {}_0\mathbf{e}_{\mathrm{N}}^*, \tag{48}$$

in which ${}_0\mathbf{e}_{\mathrm{L}}^*$ and ${}_0\mathbf{e}_{\mathrm{N}}^*$ are defined by Eqs. (33) and (35), respectively. Also, the incremental displacements, $\mathbf{u}_0^*$, and the incremental rotations, $\boldsymbol{\theta}_0^*$, are evaluated in the preceding time step.

Using the interpolation functions for the displacements and rotations given in Eq. (32) and utilizing the matrix form of strain–displacement relations given in Eq. (33), the linear part of the incremental resultant strain vector, ${}_0\mathbf{e}_{\mathrm{L}}^*$, is written as

$${}_0\mathbf{e}_{\mathrm{L}}^* = \begin{bmatrix} \mathbf{B}_u & \mathbf{B}_\theta \end{bmatrix} \begin{bmatrix} \bar{\mathbf{N}}_u & \mathbf{N}_c \\ \mathbf{N}_\theta & \mathbf{0} \end{bmatrix} \begin{Bmatrix} \mathbf{v}^* \\ \mathbf{v}_c^* \end{Bmatrix}. \tag{49}$$

The nonlinear incremental resultant strain vector, ${}_0\mathbf{e}_N^*$, contains the terms associated with the in-plane deformations, i.e.,

$${}_0\mathbf{e}_{\mathrm{N}}^{*T} = \left\{ {}_0\mathbf{e}_{\epsilon\mathrm{N}}^{*T}, \mathbf{0}^T, \mathbf{0}^T \right\}, \tag{50}$$

where the vector ${}_0\mathbf{e}_{\epsilon\mathrm{N}}^*$ ($= 1/2\boldsymbol{\varepsilon}^{*T}\mathscr{D}^{*T}$) is defined in Eq. (35) in sub-matrix form. Similar to the linear incremental strain component, the finite element representation of the vector ${}_0\mathbf{e}_{\epsilon\mathrm{N}}^*$ is achieved by combining Eqs. (32) and (50) as

$$ {}_0\mathbf{e}^*_{\mathrm{cN}} = \frac{1}{2}\left[\mathfrak{v}^{*T}\ \mathfrak{v}^{*T}_c\right]\begin{bmatrix}\mathfrak{N}^T_u\\ \mathfrak{N}^T_c\end{bmatrix}\mathfrak{B}^T\mathfrak{B}\left[\bar{\mathbf{N}}_u\ \mathbf{N}_c\right]\begin{Bmatrix}\mathbf{v}^*\\ \mathbf{v}^*_c\end{Bmatrix}, \tag{51} $$

where the matrices $\mathfrak{v}^*$, $\mathfrak{v}^*_c$, $\mathfrak{N}_u$, $\mathfrak{N}_c$, and $\mathfrak{B}$ are defined as

$$ \mathfrak{v}^* = \begin{bmatrix}\mathbf{v}^* & \mathbf{0} & \mathbf{0}\\ \mathbf{0} & \mathbf{v}^* & \mathbf{0}\\ \mathbf{0} & \mathbf{0} & \mathbf{v}^*\end{bmatrix}, $$

$$ \mathfrak{v}^*_c = \begin{bmatrix}\mathbf{v}^*_c & \mathbf{0} & \mathbf{0}\\ \mathbf{0} & \mathbf{v}^*_c & \mathbf{0}\\ \mathbf{0} & \mathbf{0} & \mathbf{v}^*_c\end{bmatrix}, $$

$$ \mathfrak{N}_u = \begin{bmatrix}\bar{\mathbf{N}}_u & \mathbf{0} & \mathbf{0}\\ \mathbf{0} & \bar{\mathbf{N}}_u & \mathbf{0}\\ \mathbf{0} & \mathbf{0} & \bar{\mathbf{N}}_u\end{bmatrix}, $$

$$ \mathfrak{N}_c = \begin{bmatrix}\mathbf{N}_c & \mathbf{0} & \mathbf{0}\\ \mathbf{0} & \mathbf{N}_c & \mathbf{0}\\ \mathbf{0} & \mathbf{0} & \mathbf{N}_c\end{bmatrix} $$

and

$$ \mathfrak{B} = \begin{bmatrix}\mathbf{I}\dfrac{\partial}{\partial x} & 0 & \mathbf{I}\dfrac{\partial}{\partial y}\\ 0 & \mathbf{I}\dfrac{\partial}{\partial y} & \mathbf{I}\dfrac{\partial}{\partial x}\end{bmatrix}. $$

The matrix differential operator, $\mathfrak{B}$, is given in Eq. (40).

Known incremental nodal displacement vectors, $\mathbf{v}^*$ and $\mathbf{v}^*_c$, from the preceding time step permit the computation of the linear and nonlinear incremental resultant strain vectors, ${}_0\mathbf{e}^*_{\mathrm{L}}$ and ${}_0\mathbf{e}^*_{\mathrm{N}}$, from Eqs. (49) and (51), respectively. Although the incremental nodal displacement vectors are determined from the equations of equilibrium, the direct utilization of these vectors to Eqs. (49) and (51) may cause difficulties and even deterioration of computed results from their actual values. This is mainly due to the incremental rotations, which can easily violate vector operations when they become large in magnitude. An in-depth discussion on finite rotations and a single pseudo vector representation of a set of consecutive rotations can be found in the paper by Argyris (1982). Therefore, the components of $\mathbf{v}^*$ and $\mathbf{v}^*_c$ must be treated in a different way in order to compute the strains and stresses accurately. In the nonlinear finite element analysis of plates and shells, a common approach to handling large rotations and to simplifying the computation of internal forces is to employ a co-rotational (moving or convected) coordinate system. Argyris et al. (1964) and Wempner (1969) are among the early investigators who applied the convected co-ordinate system to the solution of nonlinear static problems; Belytschko and Hsieh (1973) also successfully employed the same approach to the solution of nonlinear dynamic problems.

In the co-rotational formulation, a moving Cartesian co-ordinate system containing the initial configuration of an element is rigidly tied to the element. The configuration of the element described in this coordinate system may be called the ghost configuration. As the actual element deforms, the ghost

configuration follows the element as a rigid-body. Thus, the distance between the deformed element and the undeformed rigid ghost element is a measure of the actual deformations. The incremental strains given in Eqs. (49) and (51) can then be computed, once the deformational part of the element displacements is extracted from the total displacements of the element, because the rigid-body part of the displacements do not create strains and stresses. In this analysis, the deformational parts of the incremental displacements and rotations, represented by $(\mathbf{v}_d^*, \mathbf{v}_{dc}^*)$, are extracted from the total incremental displacements and rotations, $(\mathbf{v}^*, \mathbf{v}_c^*)$, by utilizing the methods proposed by Bathe and Ho (1981) for the deformational displacements and by Rankin and Brogan (1986) for the deformational rotations. In the computation of the incremental strains Eq. (48) and incremental stresses Eq. (47), the vectors $(\mathbf{v}_d^*, \mathbf{v}_{dc}^*)$ are used in place of the incremental nodal vectors $(\mathbf{v}^*, \mathbf{v}_c^*)$. Therefore, with the resultant stresses known from Eq. (47), the generation of the geometric stiffness matrix $\mathbf{k}_{\sigma ij}$ and the internal force vector $(\mathbf{f}_\sigma, \mathbf{f}_{\sigma c})$ is completed.

Unlike the incremental resultant stress vector ${}_0\boldsymbol{\sigma}^*$, computation of the resultant thermal stress vector is straightforward because a direct relation between the thermal stresses and the applied temperature can be established, regardless of the magnitude of the displacements or deformations. In this analysis, the temperature distribution over the surface and across the thickness of the element is assumed to be linear:

$$T(x, y, \bar{z}) = \frac{1}{2}T^{(+)}(x, y)\left(1 + \frac{2\bar{z}}{H}\right) + \frac{1}{2}T^{(-)}(x, y)\left(1 - \frac{2\bar{z}}{H}\right), \tag{52}$$

with

$$\left\{ \begin{array}{c} T^{(+)}(x, y) \\ T^{-}(x, y) \end{array} \right\} = \xi_1 \left\{ \begin{array}{c} T_1^{(+)} \\ T_1^{(-)} \end{array} \right\} + \xi_2 \left\{ \begin{array}{c} T_2^{(+)} \\ T_2^{(-)} \end{array} \right\} + \xi_3 \left\{ \begin{array}{c} T_3^{(+)} \\ T_3^{(-)} \end{array} \right\}. \tag{53}$$

In Eq. (53), the temperature distributions over the upper and lower faces of the element are represented by the temperature field functions $T^{(+)}(x, y)$ and $T^{(-)}(x, y)$, respectively. These functions are also approximated linearly in terms of temperatures at the nodal points by using the area coordinates ζ_1, ζ_2 and ζ_3, which are given in Appendix A.

Based on the assumption that the material properties are independent of the temperature change, the relation between the thermal stress vector, ${}_0^{t+\Delta t}\boldsymbol{\tau}$, and the applied temperature, ${}^{t+\Delta t}T$ as defined by Eq. (52), can be written as

$${}_0^{t+\Delta t}\boldsymbol{\tau} = \frac{1}{2}\mathbf{Q}^{(k)}\boldsymbol{\alpha}^{(k)}\left[{}^{t+\Delta t}T^{(+)}(x, y)\left(1 + \frac{2\bar{z}}{H}\right) + T^{(-)}(x, y)\left(1 - \frac{2\bar{z}}{H}\right)\right], \tag{54}$$

in which the vector $\boldsymbol{\alpha}^{(k)}$ contains the thermal expansion coefficients of the k^{th} layer defined with respect to the element coordinate system in the form

$$\boldsymbol{\alpha}^{(k)T} = \left\{\alpha_{xx}^{(k)}, \alpha_{yy}^{(k)}, \alpha_{xy}^{(k)}, 0, 0\right\}. \tag{55}$$

The material property matrix for the k^{th} lamina is also used in Eq. (18) for the construction of material properties relating the components of the incremental resultant stress vector ${}_0\hat{\boldsymbol{\sigma}}$ to those of the incremental resultant strain vector, ${}_0\mathbf{e}$.

Substituting from Eq. (54) for the terms involving ${}_0^{t+\Delta t}\boldsymbol{\tau}$ in Eq. (13) and carrying out the integration along the vertical direction, $\bar{z}$, gives the relation between the resultant thermal stress vector, ${}_0^{t+\Delta t}\hat{\boldsymbol{\tau}}$, and the applied temperature, ${}^{t+\Delta t}T$. The resulting expressions for ${}_0^{t+\Delta t}\hat{\boldsymbol{\tau}}$ can then be written as

$$ {}_0^{t+\Delta t}\hat{\boldsymbol{\tau}} = \boldsymbol{\Lambda}^{(+)\ t+\Delta t}T^{(+)} + \boldsymbol{\Lambda}^{(-)\ t+\Delta t}T^{(-)}, \tag{56} $$

where $\boldsymbol{\Lambda}^{(+)}$ and $\boldsymbol{\Lambda}^{(-)}$ are, respectively,

$$ \boldsymbol{\Lambda}^{(+)T} = \left\{ \boldsymbol{\Lambda}_{\epsilon}^{(+)T},\ \boldsymbol{\Lambda}_{\kappa}^{(+)T},\ \mathbf{0}^T \right\}, \tag{57} $$

with

$$ \boldsymbol{\Lambda}_{\epsilon}^{(+)} = \frac{1}{2}\sum_{k=1}^{K} \mathbf{Q}^{(k)}\boldsymbol{\alpha}^{(k)}\left[(\bar{z}_k - \bar{z}_{k-1}) + \frac{1}{H}\left(\bar{z}_k^2 - \bar{z}_{k-1}^2\right) \right], \tag{58a} $$

$$ \boldsymbol{\Lambda}_{k}^{(+)} = \frac{1}{2}\sum_{k=1}^{K} \mathbf{Q}^{(k)}\boldsymbol{\alpha}^{(k)}\left[\frac{1}{2}\left(\bar{z}_k^2 - \bar{z}_{k-1}^2\right) + \frac{2}{3H}\left(\bar{z}_k^3 - \bar{z}_{k-1}^3\right) \right] \tag{58b} $$

and

$$ \boldsymbol{\Lambda}^{(-)T} = \left\{ \boldsymbol{\Lambda}_{\epsilon}^{(-)T},\ \boldsymbol{\Lambda}_{\kappa}^{(-)T},\ \mathbf{0}^T \right\}, \tag{59} $$

with

$$ \boldsymbol{\Lambda}_{\epsilon}^{(-)} = \frac{1}{2}\sum_{k=1}^{K} \mathbf{Q}^{(k)}\boldsymbol{\alpha}^{(k)}\left[(\bar{z}_k - \bar{z}_{k-1}) - \frac{1}{H}\left(\bar{z}_k^2 - \bar{z}_{k-1}^2\right) \right] \tag{60a} $$

and

$$ \boldsymbol{\Lambda}_{\kappa}^{(-)} = \frac{1}{2}\sum_{k=1}^{K} \mathbf{Q}^{(k)}\boldsymbol{\alpha}^{(k)}\left[\frac{1}{2}\left(\bar{z}_k^2 - \bar{z}_{k-1}^2\right) - \frac{2}{3H}\left(\bar{z}_k^3 - \bar{z}_{k-1}^3\right) \right]. \tag{60b} $$

Finally, for a specified temperature distribution, ${}^{t+\Delta t}T$ in the form of Eqs. (52) and (53), substituting from Eq. (56) for the resultant thermal stress vector, ${}_0^{t+\Delta t}\hat{\boldsymbol{\tau}}$, in Eq. (37) and following through Eqs. (41a) and (41b) complete the formulation of the geometric stiffness matrix arising from thermal loading.

In the derivation of the thermal loading vector, $(\mathbf{f}_{\tau},\ \mathbf{f}_{\tau c})$, the thermal stress vectors, ${}_0^{t+\Delta t}\hat{\boldsymbol{\tau}}^{(+)}$ and ${}_0^{t+\Delta t}\hat{\boldsymbol{\tau}}^{(-)}$, are defined in the form

$$ {}_0^{t+\Delta t}\hat{\boldsymbol{\tau}}^{(+)} = \boldsymbol{\Lambda}^{(+)\ t+\Delta t}T^{(+)} \tag{61a} $$

and

$$ {}_0^{t+\Delta t}\hat{\boldsymbol{\tau}}^{(-)} = \boldsymbol{\Lambda}^{(-)\ t+\Delta t}T^{(-)}. \tag{61b} $$

Using these relations, the resultant thermal stress vector, ${}_0^{t+\Delta t}\hat{\boldsymbol{\tau}}$, can be decomposed as

$$ {}_0^{t+\Delta t}\hat{\boldsymbol{\tau}} = {}_0^{t+\Delta t}\hat{\boldsymbol{\tau}}^{(+)} + {}_0^{t+\Delta t}\hat{\boldsymbol{\tau}}^{(-)}. \tag{62} $$

Similarly, using Eq. (62), the thermal loading vector, $(\mathbf{f}_{\tau},\ \mathbf{f}_{\tau c})$, can be decomposed as

$$ \begin{Bmatrix} \mathbf{f}_{\tau} \\ \mathbf{f}_{\tau c} \end{Bmatrix} = \begin{Bmatrix} \mathbf{f}_{\tau}^{(+)} \\ \mathbf{f}_{\tau c}^{(+)} \end{Bmatrix} + \begin{Bmatrix} \mathbf{f}_{\tau}^{(-)} \\ \mathbf{f}_{\tau c}^{(-)} \end{Bmatrix}, \tag{63} $$

with

$$\mathbf{f}_{\tau}^{(+)} = \int_{{}^0A} \left(\bar{\mathbf{N}}_u^T \mathbf{B}_u^T + \mathbf{N}_\theta^T \mathbf{B}_\theta^T\right) \mathbf{\Lambda}^{(+)\ t+\Delta t} T^{(+)}\, \mathrm{d}\,{}^0A, \tag{64a}$$

$$\mathbf{f}_{\tau c}^{(+)} = \int_{{}^0A} \mathbf{N}_c^T \mathbf{B}_c^T \mathbf{\Lambda}^{(+)\ t+\Delta t} T^{(+)}\, \mathrm{d}\,{}^0A, \tag{64b}$$

$$\mathbf{f}_{\tau}^{(-)} = \int_{{}^0A} \left(\bar{\mathbf{N}}_u^T \mathbf{B}_u^T + \mathbf{N}_\theta^T \mathbf{B}_\theta^T\right) \mathbf{\Lambda}^{(-)\ t+\Delta t} T^{(-)}\, \mathrm{d}\,{}^0A \tag{64c}$$

and

$$\mathbf{f}_{\tau c}^{(-)} = \int_{{}^0A} \mathbf{N}_c^T \mathbf{B}_c^T \mathbf{\Lambda}^{(-)\ t+\Delta t} T^{(-)}\, \mathrm{d}\,{}^0A. \tag{64d}$$

2.4. External virtual work

The virtual work due to external nodal and traction forces in the k^{th} element is expressed as

$$\delta \mathscr{W}^{\mathrm{e}} = \begin{Bmatrix} \delta \mathbf{v} \\ \delta \mathbf{v}_c \end{Bmatrix} + \begin{Bmatrix} \mathbf{f}_e \\ \mathbf{f}_{ec} \end{Bmatrix}, \tag{65}$$

in which

$$\mathbf{f}_e = \mathbf{f}_e^{(\mathrm{nodal})} + \int_{{}^0A} \mathbf{N}_u^T \mathscr{P}\, \mathrm{d}\,{}^0A \tag{66a}$$

and

$$\mathbf{f}_{ec} = \mathbf{f}_{ec}^{(\mathrm{nodal})} + \int_{{}^0A} \mathbf{N}_{uc}^T \mathscr{P}\, \mathrm{d}\,{}^0A, \tag{66b}$$

with

$$\mathscr{P}^T = \{0,\ 0,\ \mathscr{P}_z\}. \tag{67}$$

In this analysis, only the externally applied pressure, $\mathscr{P}_{\mathbf{z}}$, is considered in the traction vector, $\mathscr{P}$.

3. Incremental equilibrium equations

Substituting Eqs. (65), (34), (41a), (41b), (2) and (44) in the form of Eq. (63) into the statement of virtual work Eq. (17) and requiring the virtual displacements to be arbitrary result in

$$\begin{bmatrix} \mathbf{k}_{T11} & \mathbf{k}_{T12} \\ \mathbf{k}_{T12}^T & \mathbf{k}_{T22} \end{bmatrix} \begin{Bmatrix} \mathbf{v} \\ \mathbf{v}_c \end{Bmatrix} = \begin{Bmatrix} \mathbf{f}_e \\ \mathbf{f}_{ec} \end{Bmatrix} - \begin{Bmatrix} \mathbf{f}_\sigma \\ \mathbf{f}_{\sigma c} \end{Bmatrix} + \begin{Bmatrix} \mathbf{f}_{\tau}^{(+)} \\ \mathbf{f}_{\tau c}^{(+)} \end{Bmatrix} + \begin{Bmatrix} \mathbf{f}_{\tau}^{(-)} \\ \mathbf{f}_{\tau c}^{(-)} \end{Bmatrix}, \tag{68}$$

in which $\mathbf{k}_{Tij}$ form the tangential stiffness matrix defined by

$$\mathbf{k}_{Tij} = \mathbf{k}_{Lij} + \mathbf{k}_{\sigma ij} - \mathbf{k}_{\tau ij} \ (i, j = 1, 2). \tag{69}$$

4. Numerical results

The accuracy of this element is validated by modeling a previously considered cylindrically curved laminate subjected to a uniform temperature distribution as shown in Fig. 3(a). The geometric dimensions and the material properties are the same as those used by Huang and Tauchert (1991). The planform dimensions, L and W, are both equal to 160 cm. The panel thickness, H, and the radius of curvature, R, are equal to 0.8 cm and 800 cm, respectively. Each lamina forming the panel has the material properties $E_1 = 138$ GPa, $E_2 = 8.28$ Gpa, $G_{12} = 6.9$ GPa, $\nu_{12} = 0.33$, $\alpha_L = 0.18 \times 10^{-6}/^\circ$C and $\alpha_2 = 27 \times 10^{-6}/^\circ$C. Due to the presence of symmetry, only a quarter of the panel is modeled, with boundary conditions specified as

Along symmetry line ($x = W/2$): $u = w_{,x} = 0$
Along symmetry line ($y = L/2$): $v = w_{,y} = 0$
Along the edges ($x = W$, $y = L$): $u = v = w = 0$.

A comparison of the results describing the relationship between temperature and deflection at two different locations for a specially orthotropic, thick, curved panel is given in Fig. 3(b). As can be seen, the comparison reflects close agreement between these two analyses.

The capability of the present shell element under non-uniform temperature distributions is demonstrated by considering a simply supported flat laminate with/without a hole subjected to a non-uniform through-the-thickness temperature distribution, as shown in Fig. 4. In this figure, the plate has square planform dimensions, with $L = W = 0.254$ m. The simply supported boundary conditions along the horizontal and vertical edges are given as

Along the horizontal edges ($y = \pm L/2$): $u = v = w = \theta_y = 0$
Along the vertical edges ($x = \pm W/2$): $w = \theta_x = 0$.

The panel is made up of a quasi-isotropic laminate, with stacking sequence given as $[+45^\circ/-45^\circ/0^\circ/90^\circ]_{2S}$, where the fiber orientation of each layer is denoted by θ and measured with respect to the y-axis, as shown in Fig. 4. The material properties of each layer are specified as $E_1 = 130.3$ Gpa, $E_2 = 9.377$ Gpa, $G_{12} = 4.502$ Gpa, $\nu_{12} = 0.33$, $\alpha_1 = 0.139 \times 10^{-6}/^\circ$C and $\alpha_2 = 9 \times 10^{-6}/^\circ$C. Also, each layer has an equal thickness of $t_k = 0.127$ mm.

The temperature distributions on the upper and lower faces of the panel are considered to be uniform and are denoted as T_u and T_b, respectively. Assuming a linear temperature variation through the thickness of the panel, the temperature distribution at any point in the panel can be given by

$$T(x, y, \bar{z}) = \frac{1}{2}\left(1 + \frac{2\bar{z}}{H}\right)T_u + \frac{1}{2}\left(1 - \frac{2\bar{z}}{H}\right)T_b,$$

where H is the half thickness ($t_k \times 8$) of the panel.

In order to investigate the panel response for varying values of T_u and T_b, the following parameter substitutions are used:

$$\beta = \frac{T_u}{T_b} \text{ and } \lambda_0 = \frac{T_u + T_b}{2},$$

where β is a constant parameter. Note that

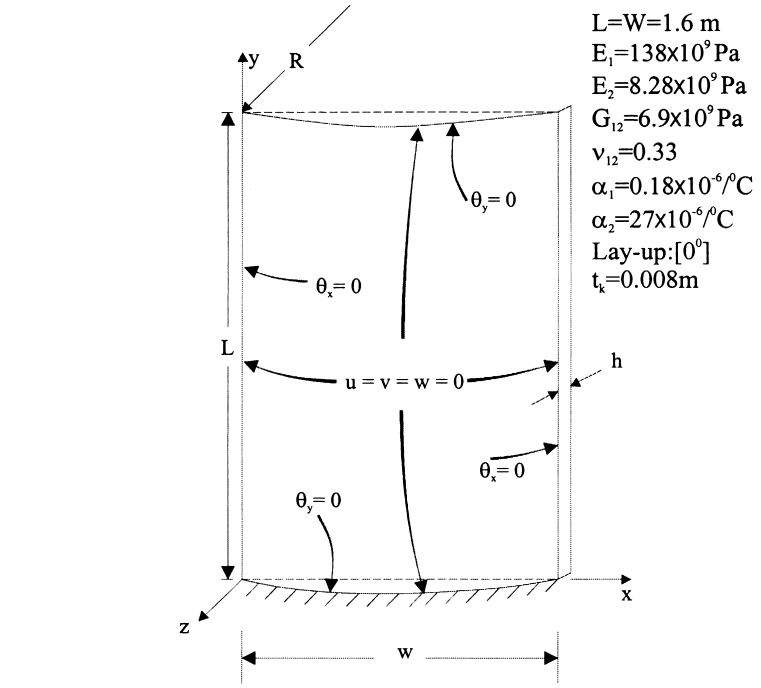

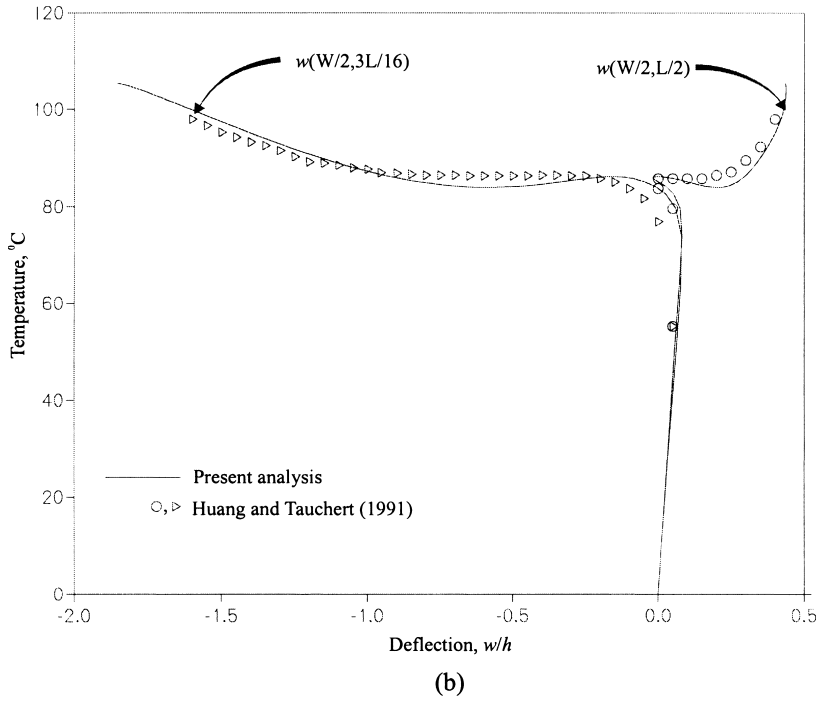

Fig. 3. Cylindrical laminate subjected to uniform thermal loading: (a) geometry and material properties and (b) comparison of results.

$$\frac{T_u}{T_b} = 0 \Longrightarrow T_u = 0 \text{ and } T_b \neq 0,$$

$$\frac{T_u}{T_b} = \infty \Longrightarrow T_u \neq 0 \text{ and } T_b = 0$$

and

$$\frac{T_u}{T_b} = 1 \Longrightarrow T_u = T_b \text{ (uniform temperature increase).}$$

The effect of non-uniform through-the-thickness temperature variation is investigated by considering the panel (a) without a cutout and (b) with a concentric circular cutout with radius $r = 0.3W$. Fig. 5 shows applied temperature at the mid-surface, λ_0, versus the out-of-plane deflections measured (a) at the center of the panel without a hole and (b) at ($x = 0$, $y = r$) of the panel with a hole. As can be seen, both cases (a) and (b) yield the same trend in their load–deflection paths. As β approaches 1, the panel response in both cases is close to bifuraction behavior (at $\beta = \beta_{cr} = 1$, there is bifurcation in both cases). Near $\beta = 0$ and $\beta = \infty$, the softening/stiffening type of large-deflection behavior is taken over by the stiffening behavior, as expected. In the case of the panel with a hole, the critical buckling temperature increases slightly.

In the next demonstration problem, a cylindrically curved, angle-ply laminate subjected to non-uniform thermal loading is considered. The geometric dimensions and the material properties of the panel are shown in Fig. 6. The simply supported boundary conditions are as follows:

Along the horizontal edges ($y = 0$ and L): $v = w = \theta_y = 0$
Along the vertical edges ($x = 0$ and w): $w = \theta_x = 0$.

Also, the horizontal movement of the panel at $x = w/2$ and $y = 0$ is suppressed in order to prevent rigid-body translation of the panel in the horizontal direciton. The temperature distributions on the

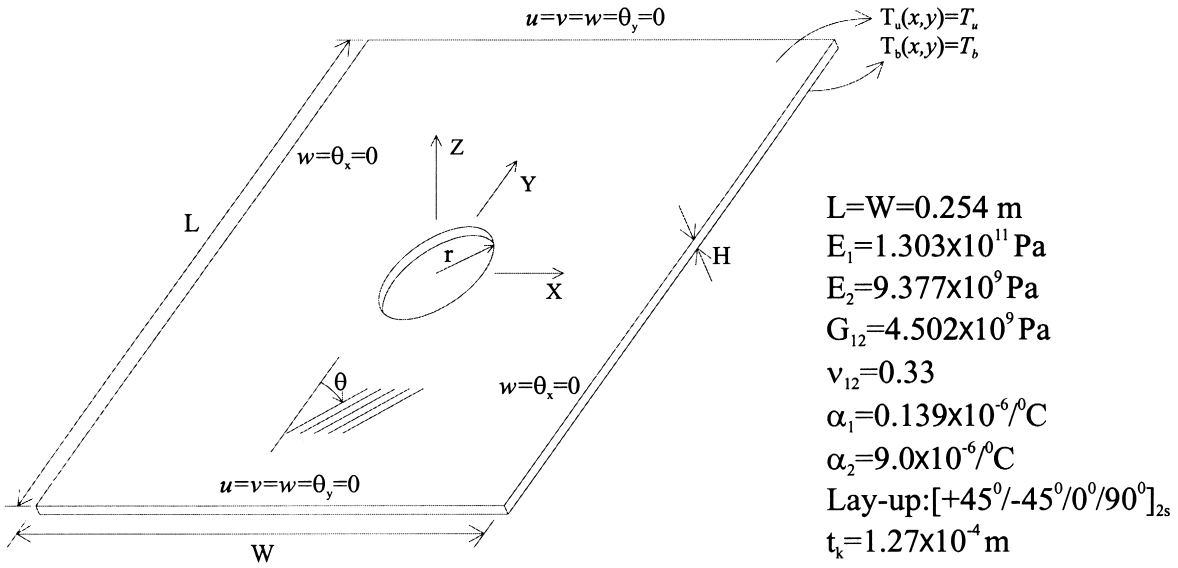

Fig. 4. Flat laminate with/without a hole under non-uniform through-the-thickness temperature distribution.

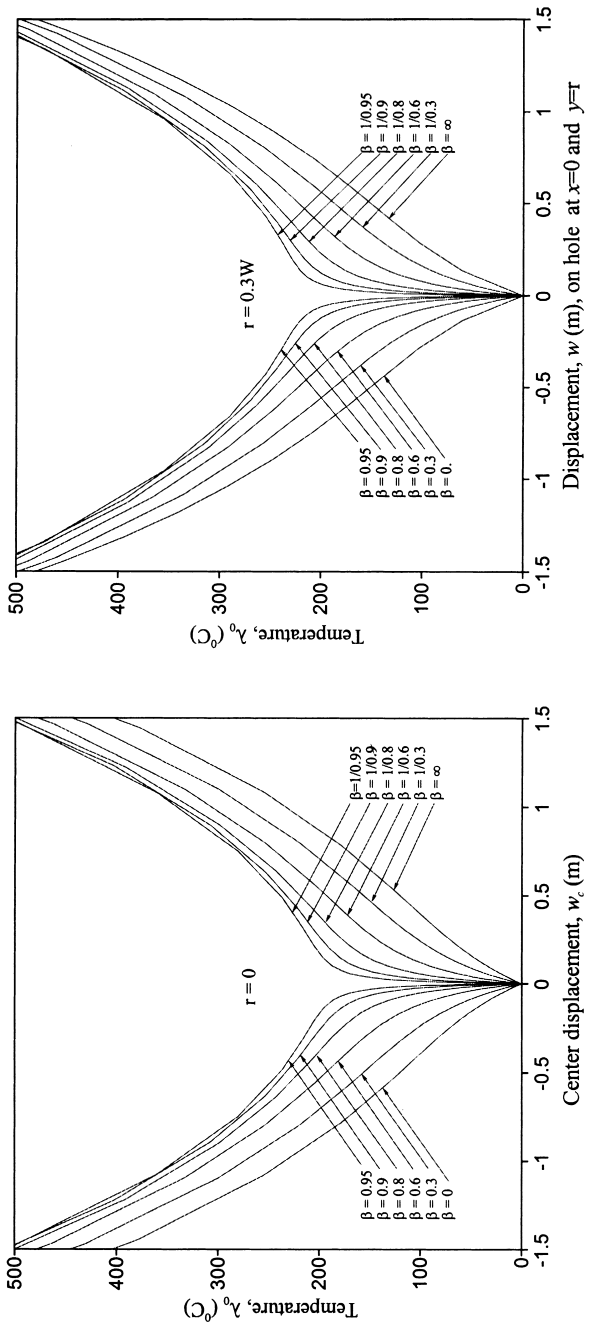

Fig. 5. Effect of non-uniform temperature distribution on the response of the flat laminate with (a) $r = 0$ and (b) $r = 0.3W$.

upper and lower faces of the panel are considered to be in the form of one-term double-sinosoidal functions with magnitudes T_u and T_b, respectively. Hence, at any point, the through-the-thickness temperature distribution is obtained from

$$T(x, y, \bar{z}) = \frac{1}{2}\left(1 - \frac{2\bar{z}}{H}\right)T_u(x, y) + \frac{1}{2}\left(1 + \frac{2\bar{z}}{H}\right)T_b(x, y).$$

The panel's nonlinear response under non-uniform temperature distributions is investigated by employing the same parameters, β and λ_0, as defined in the preceding example. Furthermore, the effect of curvature is studied by considering the panel with radii of curvatures (a) $R = 20W$ and (b) $R = 5W$, where W is the projected width of the panel on the $(X–Y)$ plane. For different values of β ranging from 0 to ∞, the plots for applied temperature, λ_0, versus the out-of-plane displacement measured at the center $(x = W/z,\ y = L/z)$ of the panel for both cases are illustrated in Fig. 7. It can be clearly seen by comparing Fig. 7(a and b) that the curvature of the panel significantly influences the panel's response. In addition, the responses before and after β_{cr} (β at which bifurcation occurs) are unsymmetric in comparison to the symmetric response of the flat plate observed in the preceding example. In Fig. 7(a), β_{cr} for the shallow panel ($R = 20W$) is between 0.675 and 0.68. The response beyond β_{cr} yields upward displacement, and the panel possesses a behavior stiffer than the panel at $\beta < \beta_{cr}$.

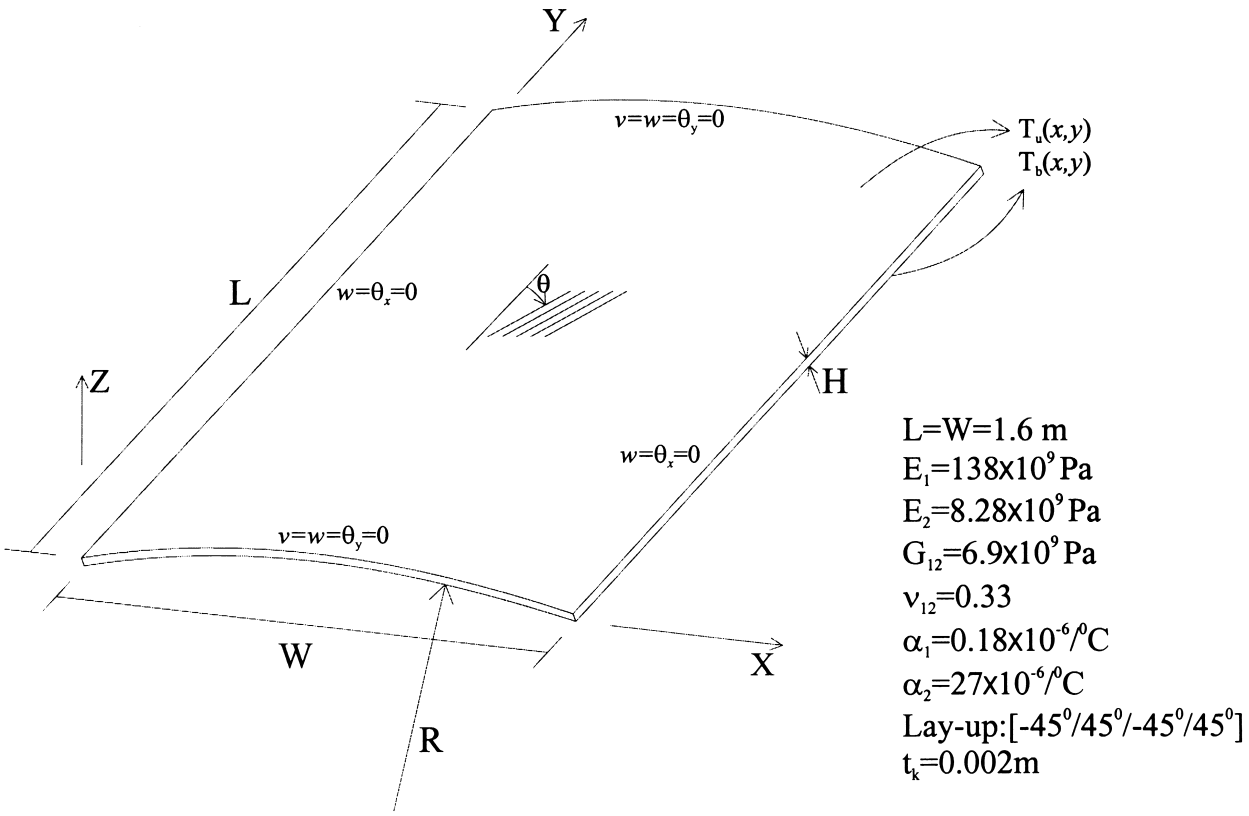

Fig. 6. Cylindrical laminate subjected to non-uniform temperature distribution.

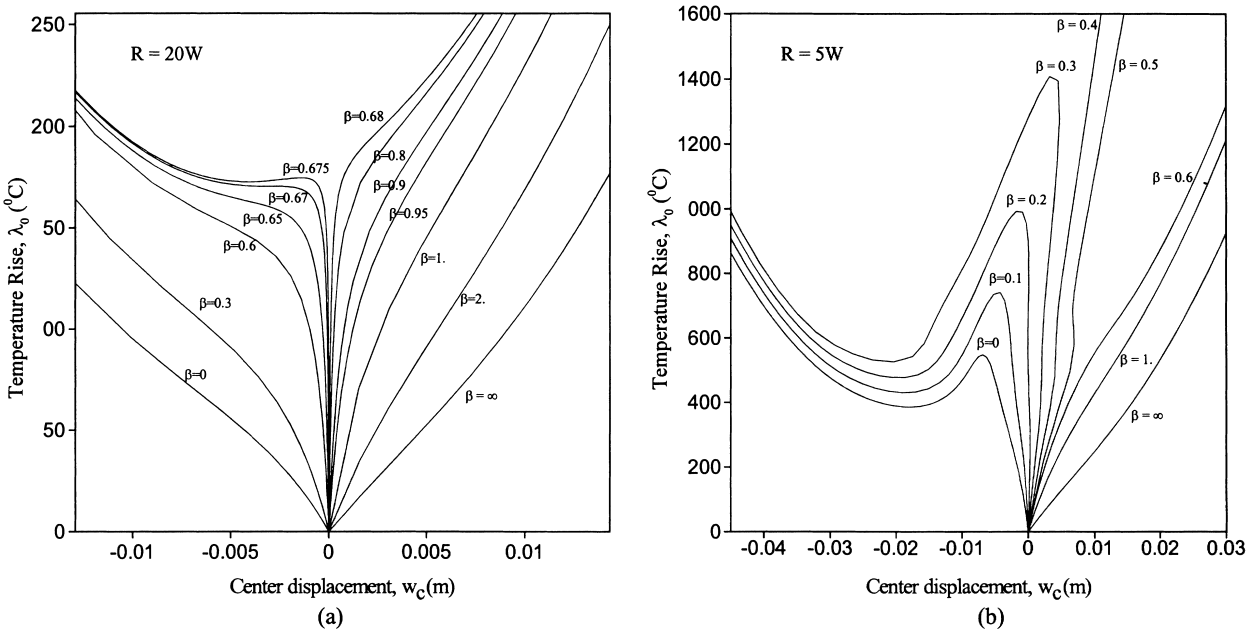

Fig. 7. Effect of curvature and non-uniform through-the-thickness temperature distribution on the response of the cylindrical panel with (a) $R = 20W$ and (b) $R = 5W$.

In the case of the panel with smaller radius of curvature ($R = 5W$), the bifurcation point, β_{cr}, is observed between $\beta = 0.5$ and $\beta = 0.6$. The panel exhibits snap-through and snap-back type postbuckling behavior between $\beta = 0$ and $\beta = 0.5$. Between $\beta = 0.5$ and $\beta = 0.6$, the panel goes through either a postbuckling behavior or a large-deflection behavior. The response beyond β_{cr} is purely of the large-deflection type.

5. Conclusions

In this analysis, the effects of non-uniform temperature variation across the shell surface and through the thickness of flat and curved laminates have been investigated by a nonlinear FE analysis. Defining a constant parameter, β, as the ratio between the thermal loads on the upper and lower faces of the panel, a series of FE analyses with the present shell element were performed to predict and understand the behavior of the panels for various values of β, along with different hole sizes and radii of curvatures of curved panels.

For flat panels, the non-uniform temperature variation resulted in a stiffening/ softening type of large-deflection response. The responses between $\beta = 0$ and $\beta = 1$ and between $\beta = 1$ and $\beta = \infty$ were the same in magnitude, but opposite in direction (the bifurcation was at $\beta = \beta_{cr} = 1$). The hole size had little effect on the responses and no effect on the deflection patterns.

For curved panels, the non-uniform temperature variation resulted in large-deflection, snap-through, and snap-back phenomena. It was observed that, as the curvature of the panel increased, β_{cr} decreased and the postbuckling response between $\beta = 0$ and $\beta = 1$ changed significantly.

Appendix A

In Eq. (26), the interpolation functions $\mathscr{N}_k$, $\mathscr{M}$k and ξ_k for the triangular element given in Fig. 8 are expressed as

$$\mathscr{N}_i = \frac{1}{2}\zeta_i(3\zeta_i - 1)(3\zeta_i - 2)\ i = 1, 2, 3,$$

$$\mathscr{N}_4 = \frac{9}{2}\zeta_1\zeta_2(3\zeta_1 - 1),$$

$$\mathscr{N}_5 = \frac{9}{2}\zeta_1\zeta_2(3\zeta_2 - 1),$$

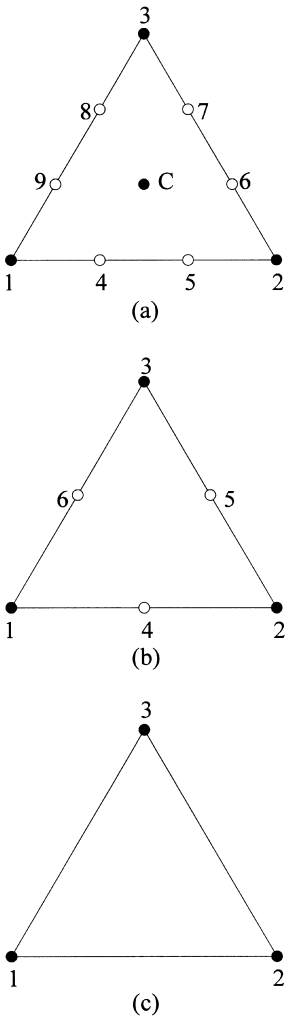

Fig. 8. Anisoparametric nodal configurations of (a) in-plane displacements, u_0 and v_0, (b) transverse displacement, w_0, and (c) out-of-plane rotations, θ_x and θ_y.

$$\mathscr{N}_6 = \frac{9}{2}\zeta_2\zeta_3(3\zeta_2 - 1),$$

$$\mathscr{N}_7 = \frac{9}{2}\zeta_2\zeta_3(3\zeta_3 - 1),$$

$$\mathscr{N}_8 = \frac{9}{2}\zeta_1\zeta_3(3\zeta_3 - 1),$$

$$\mathscr{N}_9 = \frac{9}{2}\zeta_1\zeta_3(3\zeta_1 - 1),$$

$$\mathscr{N}_c = 27\zeta_1\zeta_2\zeta_3,$$

$$\mathscr{M}_i = \zeta_i(2\zeta_i - 1)\ i = 1, 2, 3,$$

$$\mathscr{M}_4 = 4\zeta_1\zeta_2,$$

$$\mathscr{M}_5 = 4\zeta_2\zeta_3$$

and

$$\mathscr{M}_6 = 4\zeta_3\zeta_1, \tag{A1}$$

where the area parametric coordinates, ζ_i, are defined by

$$\zeta_i = \frac{1}{2A}(c_i + b_i x + a_i y),$$

in which

$$a_i = x_k - x_j;\ b_i = y_j - y_k;\ c_i = x_j y_k - y_j x_k;\ \text{and}\ A = \frac{a_3 b_2 - b_3 a_2}{2},$$

with x_i and y_i representing the coordinates of the i^{th} node of the element. In Eqs. (27a) and (27b), $\bar{\mathbf{N}}_u$, $\mathbf{N}_u^+$, $\mathbf{N}_c$ and $\mathbf{N}_\theta$ are constructed as

$$\mathbf{N}_u = \begin{bmatrix} \mathscr{N}_1 & 0 & 0 & 0 & 0 & 0 & \mathscr{N}_2 & 0 & 0 & 0 & 0 & 0 & \mathscr{N}_3 & 0 & 0 & 0 & 0 & 0 \\ 0 & \mathscr{N}_1 & 0 & 0 & 0 & 0 & 0 & \mathscr{N}_2 & 0 & 0 & 0 & 0 & 0 & \mathscr{N}_3 & 0 & 0 & 0 & 0 \\ 0 & 0 & \mathscr{M}_1 & 0 & 0 & 0 & 0 & 0 & \mathscr{M}_2 & 0 & 0 & 0 & 0 & 0 & \mathscr{M}_3 & 0 & 0 & 0 \end{bmatrix}, \tag{A2a}$$

$$\overset{+}{\mathbf{N}}_u = \begin{bmatrix} \mathscr{N}_4 & \mathscr{N}_5 & \mathscr{N}_6 & \mathscr{N}_7 & \mathscr{N}_8 & \mathscr{N}_9 & 0 & 0 & 0 & 0 & 0 & 0 & 0 & 0 & 0 \\ 0 & 0 & 0 & 0 & 0 & 0 & \mathscr{N}_4 & \mathscr{N}_5 & \mathscr{N}_6 & \mathscr{N}_7 & \mathscr{N}_8 & \mathscr{N}_9 & 0 & 0 & 0 \\ 0 & 0 & 0 & 0 & 0 & 0 & 0 & 0 & 0 & 0 & 0 & 0 & \mathscr{M}_4 & \mathscr{M}_5 & \mathscr{M}_6 \end{bmatrix}, \tag{A2b}$$

$$\mathbf{N}_c = \begin{bmatrix} \mathscr{N}_c & 0 \\ 0 & \mathscr{N}_c \\ 0 & 0 \end{bmatrix}, \tag{A2c}$$

$$\mathbf{N}_\theta = \begin{bmatrix} 0 & 0 & 0 & \zeta_1 & 0 & 0 & 0 & 0 & 0 & \zeta_2 & 0 & 0 & 0 & 0 & 0 & \zeta_3 & 0 & 0 \\ 0 & 0 & 0 & 0 & \zeta_1 & 0 & 0 & 0 & 0 & 0 & \zeta_2 & 0 & 0 & 0 & 0 & 0 & \zeta_3 & 0 \\ 0 & 0 & 0 & 0 & 0 & 0 & 0 & 0 & 0 & 0 & 0 & 0 & 0 & 0 & 0 & 0 & 0 & 0 \end{bmatrix}. \tag{A2d}$$

The matrices $\mathbf{L}_u$, $\mathbf{L}_v$, and $\mathbf{L}_w$ in Eq. (29) are expressed in the form

$$\mathbf{L}_u = \begin{bmatrix} \frac{2}{3} & 0 & 0 & \mathscr{L}^{(3)}_{11} & \mathscr{L}^{(3)}_{12} & 0 & \frac{1}{3} & 0 & 0 & \mathscr{L}^{(3)}_{13} & \mathscr{L}^{(3)}_{14} & 0 & 0 & 0 & 0 & 0 & 0 & 0 \\ \frac{1}{3} & 0 & 0 & \mathscr{L}^{(3)}_{31} & \mathscr{L}^{(3)}_{32} & 0 & \frac{2}{3} & 0 & 0 & \mathscr{L}^{(3)}_{33} & \mathscr{L}^{(3)}_{34} & 0 & 0 & 0 & 0 & 0 & 0 & 0 \\ 0 & 0 & 0 & 0 & 0 & 0 & \frac{2}{3} & 0 & 0 & \mathscr{L}^{(1)}_{11} & \mathscr{L}^{(1)}_{12} & 0 & \frac{1}{3} & 0 & 0 & \mathscr{L}^{(1)}_{13} & \mathscr{L}^{(1)}_{14} & 0 \\ 0 & 0 & 0 & 0 & 0 & 0 & \frac{1}{3} & 0 & 0 & \mathscr{L}^{(1)}_{31} & \mathscr{L}^{(1)}_{32} & 0 & \frac{2}{3} & 0 & 0 & \mathscr{L}^{(1)}_{33} & \mathscr{L}^{(1)}_{34} & 0 \\ \frac{1}{3} & 0 & 0 & \mathscr{L}^{(2)}_{13} & \mathscr{L}^{(2)}_{14} & 0 & 0 & 0 & 0 & 0 & 0 & 0 & \frac{2}{3} & 0 & 0 & \mathscr{L}^{(2)}_{11} & \mathscr{L}^{(2)}_{34} & 0 \\ \frac{2}{3} & 0 & 0 & \mathscr{L}^{(2)}_{33} & \mathscr{L}^{(2)}_{34} & 0 & 0 & 0 & 0 & 0 & 0 & 0 & \frac{1}{3} & 0 & 0 & \mathscr{L}^{(2)}_{31} & \mathscr{L}^{(2)}_{32} & 0 \end{bmatrix}, \tag{A3a}$$

$$\mathbf{L}_v = \begin{bmatrix} 0 & \frac{2}{3} & 0 & \mathscr{L}^{(3)}_{21} & \mathscr{L}^{(3)}_{22} & 0 & 0 & \frac{1}{3} & 0 & \mathscr{L}^{(3)}_{23} & \mathscr{L}^{(3)}_{24} & 0 & 0 & 0 & 0 & 0 & 0 & 0 \\ 0 & \frac{1}{3} & 0 & \mathscr{L}^{(3)}_{41} & \mathscr{L}^{(3)}_{42} & 0 & 0 & \frac{2}{3} & 0 & \mathscr{L}^{(3)}_{43} & \mathscr{L}^{(3)}_{44} & 0 & 0 & 0 & 0 & 0 & 0 & 0 \\ 0 & 0 & 0 & 0 & 0 & 0 & 0 & \frac{2}{3} & 0 & \mathscr{L}^{(1)}_{21} & \mathscr{L}^{(1)}_{22} & 0 & 0 & \frac{1}{3} & 0 & \mathscr{L}^{(1)}_{23} & \mathscr{L}^{(1)}_{24} & 0 \\ 0 & 0 & 0 & 0 & 0 & 0 & 0 & \frac{1}{3} & 0 & \mathscr{L}^{(1)}_{41} & \mathscr{L}^{(1)}_{42} & 0 & 0 & \frac{2}{3} & 0 & \mathscr{L}^{(1)}_{43} & \mathscr{L}^{(1)}_{44} & 0 \\ 0 & \frac{1}{3} & 0 & \mathscr{L}^{(2)}_{23} & \mathscr{L}^{(2)}_{24} & 0 & 0 & 0 & 0 & 0 & 0 & 0 & 0 & \frac{2}{3} & 0 & \mathscr{L}^{(2)}_{21} & \mathscr{L}^{(2)}_{22} & 0 \\ 0 & \frac{2}{3} & 0 & \mathscr{L}^{(2)}_{43} & \mathscr{L}^{(2)}_{44} & 0 & 0 & 0 & 0 & 0 & 0 & 0 & 0 & \frac{1}{3} & 0 & \mathscr{L}^{(2)}_{41} & \mathscr{L}^{(2)}_{42} & 0 \end{bmatrix}, \tag{A3b}$$

and

$$\mathbf{L}_w = \begin{bmatrix} 0 & 0 & \frac{1}{2} & \frac{b_3}{8} & -\frac{a_3}{8} & 0 & 0 & 0 & \frac{1}{2} & -\frac{b_3}{8} & \frac{a_3}{8} & 0 & 0 & 0 & 0 & 0 & 0 & 0 \\ 0 & 0 & 0 & 0 & 0 & 0 & 0 & 0 & \frac{1}{2} & \frac{b_1}{8} & -\frac{a_1}{8} & 0 & 0 & 0 & \frac{1}{2} & -\frac{b_1}{8} & \frac{a_1}{8} & 0 \\ 0 & 0 & \frac{1}{2} & -\frac{b_2}{8} & \frac{a_2}{8} & 0 & 0 & 0 & 0 & 0 & 0 & 0 & 0 & 0 & \frac{1}{2} & \frac{b_2}{8} & -\frac{a_2}{8} & 0 \end{bmatrix}, \quad \text{(A3c)}$$

with $\mathscr{L}_{mn}^{(k)}$ defined as[1]:

$$\mathscr{L}_{11} = p_1 - \cos\psi \sin\psi q_1,$$

$$\mathscr{L}_{12} = \sin^2\psi q_1,$$

$$\mathscr{L}_{13} = p_2 - \cos\psi \sin\psi q_2,$$

$$\mathscr{L}_{14} = \sin^2\psi q_2,$$

$$\mathscr{L}_{21} = \cos^2\psi q_1,$$

$$\mathscr{L}_{22} = p_1 - \cos\psi \sin\psi q_1,$$

$$\mathscr{L}_{23} = \cos^2\psi q_2,$$

$$\mathscr{L}_{24} = p_2 - \cos\psi \sin\psi q_2,$$

$$\mathscr{L}_{31} = p_3 - \cos\psi \sin\psi q_3,$$

$$\mathscr{L}_{32} = \sin^2\psi q_3,$$

$$\mathscr{L}_{33} = p_4 - \cos\psi \sin\psi q_4,$$

$$\mathscr{L}_{34} = \sin^2\psi q_4,$$

$$\mathscr{L}_{41} = \cos^2\psi q_3,$$

$$\mathscr{L}_{42} = p_3 - \cos\psi \sin\psi q_3,$$

$$\mathscr{L}_{43} = \cos^2\psi q_4$$

and

[1] For simplicity, the superscript (k) is removed, unless otherwise indicated, since all variables are defined along the k^{th} edge.

$$\mathscr{L}_{44} = p_4 - \cos\psi \sin\psi q_4, \tag{A4}$$

in which p_m and q_m are

$$p_1 = \frac{d}{9}\left(\alpha_{s1} - \frac{1}{9}\alpha_{s2}\right),$$

$$p_2 = \frac{d}{9}\left(-\alpha_{s2} + \frac{1}{9}\alpha_{s1}\right),$$

$$p_3 = \frac{d}{9}\left(\alpha_{s1} + \frac{1}{9}\alpha_{s2}\right),$$

$$p_4 = \frac{d}{9}\left(-\alpha_{s2} - \frac{1}{9}\alpha_{s1}\right),$$

$$q_1 = \frac{d}{9}\left(\alpha_{n1} + \frac{1}{9}\alpha_{n2}\right),$$

$$q_2 = \frac{d}{9}\left(-\alpha_{n2} + \frac{1}{9}\alpha_{n1}\right),$$

$$q_3 = \frac{d}{9}\left(\alpha_{n1} + \frac{1}{9}\alpha_{n2}\right)$$

and

$$q_4 = \frac{d}{9}\left(-\alpha_{n2} - \frac{1}{9}\alpha_{n1}\right), \tag{A5}$$

with

$$d^{(k)} = \sqrt{(x_j - x_i)^2 + (y_j - y_i)^2},$$

$$\alpha_{s1}^{(k)} = \cos\psi^{(k)} h_{,x}(x_i, y_i) + \sin\psi^{(k)} h_{,y}(x_i, y_i),$$

$$\alpha_{s2}^{(k)} = \cos\psi^{(k)} h_{,x}(x_j, y_j) + \sin\psi^{(k)} h_{,y}(x_j, y_j),$$

$$\alpha_{n1}^{(k)} = \sin\psi^{(k)} h_{,x}(x_i, y_i) - \cos\psi^{(k)} h_{,y}(x_i, y_i),$$

$$\alpha_{n2}^{(k)} = \sin\psi^{(k)} h_{,x}(x_j, y_j) - \cos\psi^{(k)} h_{,y}(x_j, y_j), \tag{A6}$$

$$\cos\psi^{(k)} = \frac{x_j - x_i}{d^{(k)}}$$

and

$$\sin\psi^{(k)} = \frac{y_j - y_i}{d^{(k)}}. \tag{A7}$$

The subscripts i, j, and k follow the permutation order

$i = 1, 2, 3$; $j = 2, 3, 1$ and $k = 3, 1, 2$.

In Eq. (33), the incremental strain–displacement matrix differential operators $\mathbf{B}_u$ and $\mathbf{B}_\theta$ are expressed as

$$\mathbf{B}_u = \begin{bmatrix} \dfrac{\partial}{\partial x} & 0 & 0 \\ 0 & \dfrac{\partial}{\partial y} & 0 \\ \dfrac{\partial}{\partial y} & \dfrac{\partial}{\partial x} & 0 \\ 0 & 0 & 0 \\ 0 & 0 & 0 \\ 0 & 0 & \dfrac{\partial}{\partial x} \\ 0 & 0 & \dfrac{\partial}{\partial y} \end{bmatrix} \tag{A8a}$$

and

$$\mathbf{B}_\theta = \begin{bmatrix} 0 & \dfrac{-\partial h}{\partial x} & 0 \\ -\dfrac{\partial h}{\partial y} & 0 & 0 \\ -\dfrac{\partial h}{\partial x} & -\dfrac{\partial h}{\partial y} & 0 \\ 0 & \dfrac{\partial}{\partial x} & 0 \\ \dfrac{\partial}{\partial y} & 0 & 0 \\ \dfrac{\partial}{\partial x} & \dfrac{\partial}{\partial y} & 0 \\ 0 & 1 & 0 \\ 1 & 0 & 0 \end{bmatrix}. \tag{A8b}$$

References

Argyris, J.H., 1982. An excursion into large rotations. Comp. Meth. Appl. Mech. Engng. 32, 85–155.

Argyris, J.H., Kelsey, S., Kamel, H. 1964. Matrix methods of structural analysis: A precis of recent developments. In: de Veubeke, B.F. (Ed.), Matrix Methods of Structural Analysis. Pergamon Press, New York, pp. 1–164 AGARDograph 72.

Basuli, S., 1968. Large deflections of plate problems subjected to normal pressure and heating. Indian J. Mech. Math. 6, 1–14.

Bathe, K.J., 1982. Finite Element Procedures in Engineering Analysis. Prentice–Hall, Englewood Cliffs, NJ.

Bathe, K.J., Ho, L.-W., 1981. A simple and effective element for analysis of general shell structures. Computers and Structures 13, 673–681.

Belytschko, T., Hsieh, B.J., 1973. Non-linear transient finite element analysis with convected co-ordinates. Int. J. Numer. Meth. Engng. 7, 255–271.

Berger, H.M., 1955. A new approach to the analysis of large deflections of plates. J. Applied Mechanics 22, 465–472.

Birman, V., Bert, C.W., 1993. Buckling and post-buckling of composite plates and shells subjected to elevated temperature. ASME J. Applied Mechanics 60, 514–519.

Biswas, P., 1974. Large deflection of a heated elastic circular plate under non-stationary temperature. Bull. Cal. Math. Soc. 66, 247–252.

Biswas, P., 1976. Large deflection of heated equilateral triangular plate. Indian J. Pure and Appl. Math. 7, 257–264.

Biswas, P., 1978. Large deflections of heated orthotropic plates. Indian J. Pure and Appl. Math. 9, 1027–1032.

Biswas, P., 1981. Nonlinear analysis of heated orthotropic plates. Indian J. Pure Appl. Math. 12, 1380–1389.

Chen, L.-W., Chen, L.-Y., 1989. Thermal postbuckling analysis of laminated composite plates by the finite element method. Composite Structures 12, 257–270.

Chen, L.-W., Chen, L.-Y., 1991. Thermal postbuckling behaviors of laminated composite plates with temperature-dependent properties. Composite Structures 19, 267–283.

Forray, M., Newman, M., 1962. The postbuckling analysis of heated rectangular plates. J. Aerospace Sciences 29, 1262.

Gossard, M.L., Seide, P., Roberts, W.M., 1952. Thermal Buckling of Plates NACA Technical Note, No. NACA-TN-2771.

Huang, N.N., Tauchert, T.R., 1988a. Large deformation of antisymmetric angle-ply laminates resulting from nonuniform temperature loadings. J. Thermal Stresses 11, 287–297.

Huang, N.N., Tauchert, T.R., 1988b. Postbuckling response of antisymmetric angle-ply laminates to uniform temperature loading. Acta Mechanica 72, 173–183.

Huang, N.N., Tauchert, T.R., 1991. Large deflections of laminated cylindrical and doubly-curved panels under thermal loading. Computers and Structures 41, 303–312.

von Karman, T., 1910. Festigkeitsprobleme im Maschinenbau. Encyklop. d. math. Wissensch. 4 (II), 311–385.

Librescu, L., Souza, M.A., 1991a. Thermal postbuckling behavior of geometrically imperfect shear-deformable composite flat panels. In: Singhal, S.N., Jones, W.I., Herakovich, C.T. (Eds.), Mechanics of Composites at Elevated and Cryogenic Temperatures, AMD–vol. 118. ASME, pp. 305–321.

Librescu, L., Souza, M.A. 1991b. In: Postbuckling Behavior of Shear Deformable Flat Panels under the Complex Action of Thermal and In-Plane Mechanical Loadings, pp. 917–925 AIAA Paper, No. AIAA-91-0913-CP.

Librescu, L., Souza, M.A., 1993. Post-buckling of geometrically imperfect shear deformable flat panels under combined thermal and compressive edge loadings. ASME J. Applied Mechanics 60, 526–533.

Librescu, L., Lin, W., Nemeth, M.P., Starnes, J.H.Jr. 1994. Effects of tangential edge constraints on the postbuckling behavior of flat and curved panels subjected to thermal and mechanical loads. In: Symposium, Buckling and Postbuckling of Composite Structures, ASME Winter Meeting, Chicago, ILL, November 6–11.

Librescu, L., Lin, W., Nemeth, M.P., Starnes Jr., J.H., 1995. Thermomechanical postbuckling of geometrically imperfect flat and curved panels taking into account tangential edge constraints. J. Thermal Stresses 18, 465–482.

Madenci, E., Barut, A., 1994. Thermal postbuckling analysis of cylindrically curved composite laminates with a hole. Int. J. Num. Meth. Engng. 37, 2073–2091.

Mahayni, M.A., 1966. Thermal buckling of shallow shells. Int. J. Solids Structures 2, 167–180.

Marguerre, K. 1938. Zur Theorie der gekrummten Platte grosser Formanderung. In: Fifth International Congress for Applied Mechanics, Cambridge, MA, pp. 93–101.

Meyers, C.A., Hyer, M.W. 1990. Thermal buckling and post-buckling of symmetric composite plates. In: Proceedings of the 5th Conference of the American Society of Composites, East Lansing, MI, pp. 439–448.

Meyers, C.A., Hyer, M.W., 1991. Thermal buckling and post-buckling of symmetrically laminated composite plates. Journal of Thermal Stresses 14, 519–540.

Mindlin, R.D., 1951. Influence of rotatory inertia and shear on flexural motions of isotropic, elastic plates. J. Applied Mechanics 18, 31–38.

Noor, A.K., Kim, Y.H., 1996. Buckling and postbuckling of composite panels with cutouts subjected to combined edge shear and temperature change. Computers and Structures 60, 203–222.

Noor, A.K., Peters, J.M., 1996. Nonlinear and postbuckling analyses of curved composite panels subjected to combined temperature change and edge shear. Computers and Structures 60, 853–874.

Noor, A.K., Peters, J.M., 1997. Analysis of curved sandwich panels with cutouts subjected to combined temperature gradient and mechanical loads. In: Proceedings of the ASME Aerospace Division, AD–vol. 55, pp. 293–309.

Nowinski, J.L., 1978. Theory of Thermoelasticity with Applications. Sijthoff and Noordhoff International Publishers, Alphen Aan Der Rijn, The Netherlands.

Pal, M.C., 1969. Large deflections of heated circular plates. Acta Mechanica 8, 82–103.

Pal, M.C., 1973. Static and dynamic non-linear behavior of heated orthotropic circular plates. Int. J. Non-Linear Mechanics 8, 489–504.

Powell, M.J.D., 1964. An efficient method for finding the minimum of a function of several variables without calculating derivatives. Computer J. 7, 155–162.

Raju, K.K., Rao 19, G.V., 1984a. Thermal postbuckling of circular plates. Computers and Structures 18, 1179–1182.

Raju, K.K., Rao, G.V., 1984b. Finite element analysis of thermal postbuckling of tapered columns. Computers and Structures 19, 617–620.

Raju, K.K., Rao, G.V., 1989. Thermal post-buckling of thin simply supported orthotropic square plates. Composite Structures 12, 149–154.

Rankin, C.C., Brogan, F.A., 1986. An element independent co-rotational procedure for the treatment of large rotations. J. Pressure Vessel Technology 108, 165–174.

Rao, G.V., Raju, K.K., 1984. Thermal postbuckling of columns. AIAA Journal 22, 850–851.

Reissner, E., 1945. The effect of transverse shear deformation on the bending of elastic plates. J. Applied Mechanics 12, 69–77.

Singh, G., Rao, G.V., Iyengar, N.G.R., 1993. Thermal postbuckling behavior of rectangular antisymmetric cross-ply composite plates. Acta Mechanica 98, 39–50.

Stavsky, Y., 1963. Thermoelasticity of heterogeneous aelotropic plates. J. Engineering Mechanics, Proceedings of ASCE 89 (EM2), 89–105.

Tessler, A., 1990. A C^0-anisoparametric three-node shallow shell element. Comput. Methods Appl. Mech. Engrg. 78, 89–103.

Tripathy, B., Rao, K.P., 1992. Stiffened composite cylindrical panels — optimum lay-up for buckling by ranking. Computers and Structures 42, 481–488.

Wempner, G., 1969. Finite elements, finite rotations and small strains of flexible shells. Int. J. Solids Structures 5, 117–153.

Yang, P.C., Norris, C.H., Stavsky, Y., 1966. Elastic wave propagation in heterogeneous plates. Int. J. Solids Structures 2, 665–684.